Expanding the PRAAS spectrum: *De novo* mutations of immunoproteasome subunit β-type 10 in six infants with SCID-Omenn syndrome

Graphical abstract

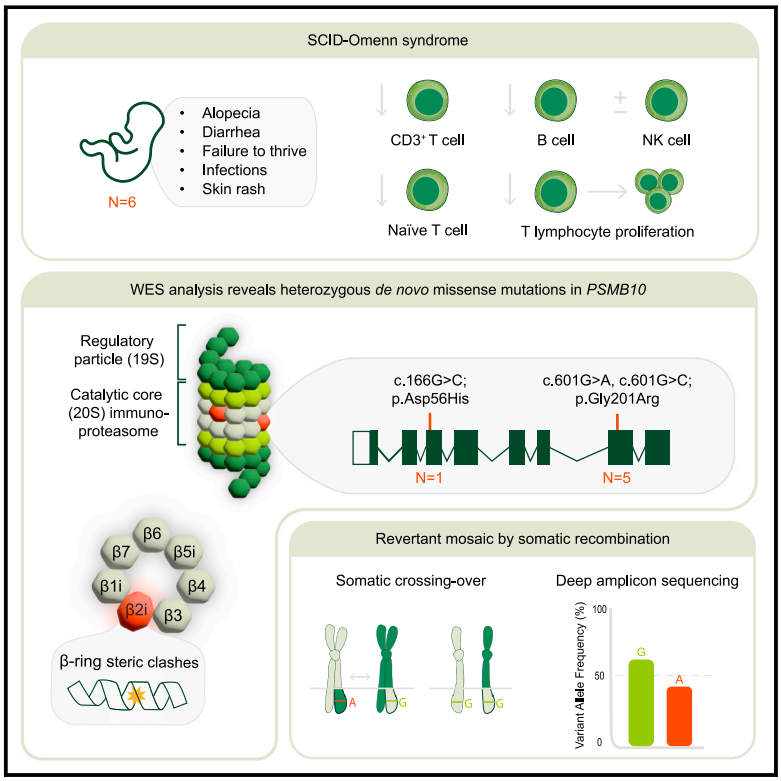

Authors

Caspar I. van der Made, Simone Kersten, Odelia Chorin, ..., Sophie Hambleton, Stefanie S.V. Henriet, Alexander Hoischen

Correspondence

alexander.hoischen@radboudumc.nl

This study highlights the identification of recurrent heterozygous *de novo* mutations in immunoproteasome subunit β2i (*PSMB10*) as a cause for SCID-Omenn syndrome. These variants are predicted to profoundly disrupt immunoproteasome structure and function, emphasizing its importance for lymphocyte development. Pathogenic variants in *PSMB10* should be sought in SCID newborn screening.

van der Made et al., 2024, The American Journal of Human Genetics *111*, 791–804
April 4, 2024 © 2024
https://doi.org/10.1016/j.ajhg.2024.02.013

Expanding the PRAAS spectrum: *De novo* mutations of immunoproteasome subunit β-type 10 in six infants with SCID-Omenn syndrome

Caspar I. van der Made,[1,2,20] Simone Kersten,[1,2,20] Odelia Chorin,[3,4,20] Karin R. Engelhardt,[5] Gayatri Ramakrishnan,[6] Helen Griffin,[5] Ina Schim van der Loeff,[5,7] Hanka Venselaar,[6] Annick Raas Rothschild,[3,4] Meirav Segev,[3] Janneke H.M. Schuurs-Hoeijmakers,[1] Tuomo Mantere,[8] Rick Essers,[9,10] Masoud Zamani Esteki,[9,10] Amir L. Avital,[11] Peh Sun Loo,[12] Annet Simons,[1] Rolph Pfundt,[1] Adilia Warris,[13,14] Marieke M. Seyger,[15] Frank L. van de Veerdonk,[2] Mihai G. Netea,[2] Mary A. Slatter,[5,7] Terry Flood,[7] Andrew R. Gennery,[5,7] Amos J. Simon,[16] Atar Lev,[16] Shirley Frizinsky,[4,16] Ortal Barel,[17] Mirjam van der Burg,[18] Raz Somech,[4,16] Sophie Hambleton,[5,7,21] Stefanie S.V. Henriet,[19,21] and Alexander Hoischen[1,2,21,*]

Summary

Mutations in proteasome β-subunits or their chaperone and regulatory proteins are associated with proteasome-associated autoinflammatory disorders (PRAAS). We studied six unrelated infants with three *de novo* heterozygous missense variants in *PSMB10*, encoding the proteasome β2i-subunit. Individuals presented with T-B-NK± severe combined immunodeficiency (SCID) and clinical features suggestive of Omenn syndrome, including diarrhea, alopecia, and desquamating erythematous rash. Remaining T cells had limited T cell receptor repertoires, a skewed memory phenotype, and an elevated CD4/CD8 ratio. Bone marrow examination indicated severely impaired B cell maturation with limited V(D)J recombination. All infants received an allogeneic stem cell transplant and exhibited a variety of severe inflammatory complications thereafter, with 2 peri-transplant and 2 delayed deaths. The single long-term transplant survivor showed evidence for genetic rescue through revertant mosaicism overlapping the affected PSMB10 locus. The identified variants (c.166G>C [p.Asp56His] and c.601G>A/c.601G>C [p.Gly201Arg]) were predicted *in silico* to profoundly disrupt 20S immunoproteasome structure through impaired β-ring/β-ring interaction. Our identification of *PSMB10* mutations as a cause of SCID-Omenn syndrome reinforces the connection between PRAAS-related diseases and SCID.

The human proteasome facilitates the controlled degradation of intracellular proteins that are targeted for breakdown by ubiquitination. The standard proteasome (SP) is composed of an enclosed cylinder-shaped central 20S core complex harboring the acidic, basic, and hydrophobic cleaving β-subunits β1, β2 ,and β5, which together with two 19S regulatory units or the PA28 regulator form the 26S proteasome.[1] The proteolytic β-subunits can be exchanged for their inducible counterparts β1i (LMP2/PSMB9), β2i (MECL1/PSMB10), and β5i (LMP7/PSMB8) to form the immunoproteasome (IP).[2] The IP is constitutively expressed in hematopoietic cells and can be induced in non-immune cells upon exposure to proinflammatory cytokines.[3] Compared to the SP, IP assembly is faster with more efficient antigen processing, explaining a fundamental role in the generation of pathogen-derived peptides and major histocompatibility complex (MHC) class I antigen presentation.[3–5] Moreover, thymic cortical epithelial cells express thymoproteasomes that are essential in establishing central tolerance, containing the β1i

[1]Department of Human Genetics, Radboud University Medical Center and Radboud Institute for Molecular Life Sciences, Nijmegen, the Netherlands; [2]Department of Internal Medicine and Radboud Center for Infectious Diseases (RCI), Radboud University Medical Centre and Radboud Institute for Molecular Life Sciences, Nijmegen, the Netherlands; [3]Institute of Rare Diseases, Edmond and Lily Safra Children's Hospital, Sheba Medical Center, Tel Hashomer, Israel; [4]Faculty of Medicine, Tel-Aviv University, Tel-Aviv, Israel; [5]Newcastle University Translational and Clinical Research Institute, Newcastle upon Tyne, UK; [6]Department of Medical BioSciences, Radboud University Medical Center, Nijmegen, the Netherlands; [7]Paediatric Immunology and Infectious Diseases, Great North Children's Hospital, Newcastle upon Tyne Hospitals NHS Foundation Trust, Newcastle upon Tyne, UK; [8]Laboratory of Cancer Genetics and Tumor Biology, Research Unit of Translational Medicine and Biocenter Oulu, University of Oulu, Oulu, Finland; [9]Maastricht University Medical Centre MUMC+, Department of Clinical Genetics, Maastricht, the Netherlands; [10]GROW School for Oncology and Developmental Biology, Department of Genetics and Cell Biology, Maastricht, the Netherlands; [11]Department of Pathology, Radboud University Medical Center, Nijmegen, the Netherlands; [12]Department of Cellular Pathology, Royal Victoria Infirmary, Newcastle upon Tyne Hospitals NHS Foundation Trust, Newcastle upon Tyne, UK; [13]MRC Centre for Medical Mycology, University of Exeter, Exeter, UK; [14]Department of Paediatric Infectious Diseases, Great Ormond Street Hospital, London, UK; [15]Department of Dermatology, Radboud University Medical Center, Nijmegen, the Netherlands; [16]Pediatric Department A and the Immunology Service, Jeffrey Modell Foundation Center, Edmond and Lily Safra Children's Hospital, Sheba Medical Center, Faculty of Medicine, Tel Aviv University, Tel-Aviv, Israel; [17]The Wohl Institute for Translational Medicine and Cancer Research Center, Sheba Medical Center, Ramat Gan, Israel; [18]Department of Pediatrics, Laboratory for Pediatric Immunology, Willem-Alexander Children's Hospital, Leiden University Medical Center, Leiden, the Netherlands; [19]Department of Pediatric Infectious Diseases and Immunology, Amalia Children's Hospital, Radboud University Medical Center, Nijmegen, the Netherlands
[20]These authors contributed equally
[21]These authors contributed equally
*Correspondence: alexander.hoischen@radboudumc.nl
https://doi.org/10.1016/j.ajhg.2024.02.013.

and β2i subunits together with the thymus-specific β5t subunit (PSMB11) instead of β5i.[6] Dysfunction of several proteasome β-subunits or their respective chaperone and regulatory proteins leads to proteasome-associated autoinflammatory syndrome (PRAAS), characterized by nodular dermatitis, lipodystrophy, recurrent fever, and type-I interferon-induced immune dysregulation.

The majority of individuals with PRAAS have underlying autosomal-recessive or digenic heterozygous mutations impairing the 20S core particle (please refer to Table 1 for an overview of PRAAS-related diseases).[7–11] Autosomal-dominant mutations in proteasome subunits or accessory proteins have been associated with phenotypes distinct from classical PRAAS. Heterozygous (*de novo*) mutations affecting 19S subunits have been described in persons with primary neurodevelopmental syndromes with a type-I interferon (IFN) signature. Moreover, individuals with *de novo* nonsense-mediated decay (NMD)-escaping mutations affecting proteasome assembly protein POMP exhibited signs of autoinflammation, immune dysregulation, and combined immunodeficiency (PRAID).[12] Recently, a recurrent *de novo* mutation in *PSMB9* was described in two infants presenting with combined immunodeficiency.[13]

Individuals with typical severe combined immunodeficiency (SCID) lack T cells altogether and present during early infancy with recurrent opportunistic infections and failure to thrive (FTT). In atypical forms of SCID, immunodeficiency is similar in severity, but the block in T cell development is incomplete, leading to low naive T cells (<20%) usually within a reduced total T cell number. Omenn syndrome (OS [MIM 603554]) is a specific form of atypical SCID, in which T cells expand oligoclonally in the periphery, infiltrating end-organs such as the skin. The clinical diagnosis of OS requires a generalized erythrodermic rash, exclusion of maternofetal engraftment, and 2 or more of hepatosplenomegaly and lymphadenopathy, eosinophilia or high IgE levels.[27] These disorders can be detected based on clinical presentation or newborn screening (NBS) programs for SCID. In this study, we describe six unrelated infants with predominant signs of SCID and clinically diagnosed Omenn(-like) syndrome who carried heterozygous *de novo* missense variants in *PSMB10*, with an overlapping revertant mosaicism (RM) in one infant. The latter individual was previously reported as part of a trio sequencing study in subjects with inborn errors of immunity (IEI).[28] Molecular modeling suggests that the encoded PSMB10 missense variants cause profound disruption of the 20S proteasome structure through impaired β-ring/β-ring interaction, similar to previously reported human mutations in *PSMB9*. These results identify *de novo* variants in *PSMB10* as a monogenic cause of autosomal-dominant SCID-OS within the spectrum of PRAAS-related diseases. All six individuals presented with early-onset erythroderma, FTT, diarrhea, alopecia, and opportunistic infections (detailed clinical history and laboratory values are available in Table 2; Figure 1A; Tables S1–S3 and Supplemental note: Case reports).

The skin rash manifested within two months after birth and was characterized as a generalized erythroderma with desquamation (individual 1 [Figure 1B], 3, and 4), a raised generalized maculopapular rash (individuals 5 and 6), or only a mild facial erythroderma diagnosed as acne neonatorum (individual 2). The infections consisted of oral candidiasis (individuals 1, 3, and 4), disseminated and chronic viral infections (varicella zoster virus [VZV]), adenovirus, cytomegalovirus (CMV) (individuals 2, 4, and 5), *Pneumocystis* pneumonia (individual 4), or secondary skin infections (individuals 1 and 4). Individuals 2 and 5 displayed severe, intractable diarrhea that required total parenteral nutrition (TPN). A sixth infant (individual 6) was identified via NBS as having low T cell receptor excision circles (TRECs) and thrived despite developing blood and mucus in his stools and generalized dry skin by 2 months of age. On laboratory testing, T lymphocytes were low in number with an elevated CD4:CD8 ratio (except individual 2) and skewing toward a memory phenotype with low CD45RA and/or elevated CD45RO expression and reduced proliferative capacity (Table 2). T cell receptor (TCR) repertoires were limited (tested in individuals 1, 2, and 3). Circulating B lymphocytes were reduced or absent, associated with marked hypogammaglobulinemia. Natural killer (NK) cell numbers were low-normal. Individuals 1–4 had hypereosinophilia, which is typical for SCID-OS. Bone marrow (BM) examination showed a near complete block of B lymphocyte development in individuals 1 and 5, although slightly less severe when compared with other individuals with OS caused by RAG1, RAG2, or Artemis deficiency (Figure S1). In individual 6, a non-accredited interferon-stimulated gene transcriptional signature was assessed pre-transplant and was not markedly raised (5 of 6 transcripts showed normal abundance while *IFI27* transcripts were 3× above the upper limit of normal).

Histological examination of the skin indicated a flattened epidermis with vacuolization of the basal epidermal layer and hyperparakeratosis in individuals 1 (Figure 1C) and 3 and vacuolar dermatitis with eosinophils and pigment laden macrophages in individual 2. Lymph node biopsy in individual 5 was stroma-rich with a paucity of ($CD4^+$) lymphocytes, abortive primary follicle formation, and absence of germinal centers (Figures 1D and S2A–S2C). Small bowel biopsies in individuals 3 and 5 showed partial villous atrophy and crypt hyperplasia with apoptotic bodies, while colon biopsies showed preserved crypt architecture (Figures 1E, 1F, S2D, and S2E). Immunohistochemistry demonstrated an empty lamina propria with lack of plasma cells, low T cell numbers, and absence of B lymphocytes, consistent with an immunodeficiency-related enteropathy (Figures 1G and S2F–S2H).

All affected infants received allogeneic hematopoietic stem cell transplantation (HSCT) with different donor types and pre-conditioning regimens (Table 2). Post-transplant outcomes were characterized by severe inflammatory complications, including graft-versus-host disease (GVHD)

Table 1. Current genetic and clinical spectrum of monogenic proteasome-associated inflammatory diseases

Gene	*PSMB8*[7,10,14–16]	*POMP*[12,17]	*PSMB4*[8,18]	*PSMG2*[9]	*PSMB10*[11,19]	*PSMB1*[20]	*PSMD12*[21–24]	*PSMC3*[,25]	*PSMC3*[26,]	*PSMB9*[13]
Disease	PRAAS1 (MIM: 256040	PRAAS2 (MIM: 618048)	PRAAS3 (MIM: 617591)	PRAAS4 (MIM: 619183)	PRAAS5 (MIM: 619175)	NDD (MIM: 620038)	Stankiewicz–Isidor syndrome (MIM: 617516)	NDD	DCIDP (MIM: 619354)	PRAAS-ID
Mutational mechanism	AR LoF	AD LoF DN	AR LoF	AR LoF	AR LoF	AR LoF	AD LoF HI	AD LoF	AR LoF	*De novo* LoF DN
Encoded protein	Subunit β5i	proteasome maturation protein	subunit β7	assembly chaperone 2	subunit β2i	subunit β6	19S/26S subunit, non-ATPase 12	19S/26S subunit, ATPase 3	19S/26S subunit, ATPase 3	subunit β1i
Proteasome defect	20S, 26S IP defect	20S, 26S IP + SP defect	20S, 26S IP + SP defect	20S, 26S IP + SP defect	20S, 26S IP defect	20S, 26S SP defect	20S IP + SP defect	20S, 26S SP + IP defect	decreased ubiquitylation, proteotoxic stress	20S IP defect
Clinical findings										
Periodic fever	+	+	+	+	+	–	–	–	–	+
Skin rash	+	+	+	+	+	–	+	–	–	+
Myositis/muscle dystrophy	+	–	+	+	–	N/A	N/A	–	–	+
Arthritis	+	+	+	–	–	–	–	–	–	–
Liver dysfunction	+	N/A	+	N/A	N/A	N/A	N/A	N/A	N/A	+
Infections	+/–	+	+	–	N/A	–	–	–	–	+
Pneumonia	+	+	+	–	–	–	–	–	–	+
Splenomegaly	+	–	+	+	+	–	–	–	–	+/–
Lipodystrophy	+	+	+	+	N/A	–	–	–	–	–
Basal ganglia calcification	+/–	–	–	+	N/A	N/A	–	N/A	N/A	+
IFN-I signature	+	++	+	+	+	N/A	+	+	N/A	=/+
Viremia	N/A	N/A	–	–	N/A	N/A	–	–	–	+
Congenital malformations (incl. facial dysmorphism)	+	+	N/A	N/A	+	++ (short stature, deafness)	+++ (deafness)	+++ (deafness)	+++ (cataract, deafness)	N/A
Neurological abnormalities	+	+	N/A	+	N/A	+++ (IDD)	+++ (ID D, autism)	+++ (IDD)	+++ (I DD, PNP)	–
Laboratory evaluation										
Elevated inflammatory markers	+	+	+	+	+	N/A	+	N/A	N/A	+
Microcytic anemia	+	N/A	+/–	–	+	N/A	N/A	N/A	N/A	N/A
Thrombocytopenia	=/↑	+	+	+	=/↑	N/A	N/A	N/A	N/A	+

(*Continued on next page*)

Table 1. *Continued*

Gene	*PSMB8*[7,10,14–16]	*POMP*[2,17]	*PSMB4*[8,18]	*PSMG2*[9]	*PSMB10*[11,19]	*PSMB1*[20]	*PSMD12*[21–24]	*PSMC3*[25]	*PSMC3*[26,]	*PSMB9*[13]
T cell	N/A	CD4 ↑, CD8 ↓, CD4/CD8 ratio ↑, naive T cell phenotype	low CD8, CD4/CD8 ratio ↑	N/A	N/A	N/A	variable	N/A	N/A	variable
B cell	N/A	↓	variable	N/A	N/A	N/A	=/↑	N/A	N/A	=/↓
Serum Ig	↑	Dysgamma-globulinemia	=/↑	N/A	normal	N/A	N/A	N/A	N/A	IgG ↓
Auto-antibodies	variable	+	+	+	N/A	N/A	N/A	N/A	N/A	–

AD, autosomal-dominant; AR, autosomal-recessive; DCIDP, deafness, cataract, impaired intellectual development, and polyneuropathy; DN, dominant-negative; HI, haploinsufficiency; IDD, intellectual and developmental disability; IFN-I, type-I interferon; LoF, loss-of-function; NDD, neurodevelopmental disorders; PNP, polyneuropathy.

in individuals 1, 3, 4, and 5 and fatal thrombotic micro-angiopathy (TMA) in individual 2. Shortly after HSCT, individual 4 died following encephalopathy caused by treatment-refractory reactivation of VZV and associated encephalitis confirmed at autopsy. Individual 6 developed an acute neurological deterioration one month after transplant with evidence of widespread white matter changes on magnetic resonance imaging and the main differential diagnosis of chemotherapy-related neurotoxicity or immune-mediated encephalitis. He improved with high-dose corticosteroids and supportive care, but the long-term neurological prognosis remains guarded. Individuals 3 and 5 had signs of severe chronic enteropathy during long-term follow up. Immunosuppressive treatment yielded a partial response in individual 5 that was complicated by chronic norovirus infection, and he died due to sepsis at age 4. Individual 3, who had learning difficulties, acquired other chronic comorbidities, including liver cirrhosis and hemodialysis-dependent end-stage renal disease and died at the age of 16. Individual 1 suffered from severe cyclosporin-related toxicity and still experiences notable infection- and drug-induced hypersensitivity, resulting in toxic skin reactions. He is currently 18 years after HSCT and has normal cognitive and intellectual development.

Clinical whole-exome sequencing (WES) was performed in all individuals, but *in silico* analysis did not reveal any actionable variants within known genes associated with IEI.[29] Written informed consent and publication consent were obtained from individuals 1–2 and/or their parents and were approved by the local ethics committees. Parents of individuals 3–6 provided generic consent for future research through ethically approved procedures (REC ref. 10/H0906/22). Subsequently, exome-wide research-based analysis identified three heterozygous missense variants in *PSMB10*: two variants affected the same nucleotide in exon 7 (c.601G>A [GenBank: NM_002801] [p.Gly201Arg] and c.601G>C [GenBank: NM_002801] [p.Gly201Arg]) and one was located in exon 3 (c.166G>C [GenBank: NM_002801] [p.Asp56His]) (Figure 1A). All variants impacted highly conserved nucleotides and amino acid residues in the protein structure. The variants were predicted by *in silico* tools to be deleterious and were absent from population and our in-house WES databases (Table 1; Figure 1H). Trio-based exome sequencing in individuals 1 and 2 and segregation analysis in individuals 3, 4, 5, and 6 determined all variants to be *de novo*, while no other disease-causing candidate variants were identified (Table S4). Using a commercial antibody, we performed immunoblotting for PSMB10 protein on dermal fibroblasts that were available from individuals 3, 4, and 5 and controls, with or without prior IFN-gamma treatment (Figure 1I). There was no difference in overall PSMB10 protein accumulation nor the ratio of immature to mature forms, but we noted an additional band of intermediate size present only in samples from individuals bearing a PSMB10 variant. This implies that mutated protein is expressed but shows altered physico-chemical characteristics, consistent with

Table 2. Genetic and clinical characteristics of individuals with monoallelic *PSMB10* variants

	Individual 1	Individual 2	Individual 3	Individual 4	Individual 5	Individual 6
Genetics						
Ancestry	European	Jewish-Sepharadi	European	European	European	European
Variant	c.601G>A (p.Gly201Arg)	c.601G>A (p.Gly201Arg)	c.601G>C (p.Gly201Arg)	c.601G>A (p.Gly201Arg)	c.166G>C (p.Asp56His)	c.601G>A (p.Gly201Arg)
Allele frequency[a]	0	0	0	0	0	0
CADD-Phred score	35	35	34	35	28	35
Clinical presentation						
Age at investigation (weeks)	8	2	6	13	4	0[c]
Sex	M	M	M	F	M	M
Failure to thrive	+	+	+	+	+	–
Diarrhea	+	+++	+	+	+++	+
Skin rash	+++	+	+++	+++	++	+
Age at onset rash (weeks)	<1	2	3	1	8	<1
Recurrent infections	+	+	+	+	+	–
Systemic inflammation	–	+	–	–	–	–
Hepatomegaly	–	–	+	+	–	–
Lymphadenopathy	+	–	–	–	+	–
Alopecia	+	+	+	+	N/A	–
Dysmorphology	+	+	–	–	–	–
Laboratory investigation[b]						
Eosinophils (/μL) (40–800)	896	2,930	1,700	1,700	720	1,000
IgG (g/L) (3.7–12.6)	1.35	0.974	2.6	2.76	5.1	2.4
IgA (g/L) (0.02–0.15)	<0.07	<0.01	<0.07	0.23	0.41	<0.04
IgM (g/L) (0.05–0.29)	<0.07	<0.02	0.09	0.12	0.98	<0.04
CD3 (/μL) (1,700–3,600)	1,300	1,552	595	1,239	188	309
CD4 (/μL) (1,700–2,800)	1,100	730	551	1,143	137	272
CD8 (/μL) (800–1,200)	40	820	72	83	26	60
CD4:CD8 ratio	27.5	0.89	7.7	13.8	5.3	4.5
CD19 (/μL) (500–1500) (%)	40	430 (cells/mm^3)	0	<1	19	34

(*Continued on next page*)

Table 2. ***Continued***

	Individual 1	Individual 2	Individual 3	Individual 4	Individual 5	Individual 6
CD3/CD56 (/μL) (300–700)	70	1,826	46	414	22	368
CD45RA (%CD3)	8.6	N/A[c]	1	0	8	0
CD45RO (%CD3)	95	N/A[c]	91	N/A	N/A	4
TCR αβ (%CD3)	98	N/A	97	99	74	96
TCR γδ (%CD3)	2	N/A	3	1	26	4
Mitogen response (PHA)	decreased	decreased	decreased	decreased	decreased	decreased
Therapy–Hematopoietic stem cell transplantation (HSCT)						
Age at transplant (weeks)	12	130	11	16	12	9
Donor information	HLA identical sibling	URD	URD cord	maternal haplo	9/10 mM cord blood	paternal haplo
Serotherapy	ATG	ATG	alemtuzumab	ATG	none	ATG + Rituximab
Chemotherapy	Cyclo	Cyclo + MMF	Flu + Mel	Bu + Cyclo	Treo + Flu	Treo + Flu
Outcome and follow up	alive, age 18 years	died, age 2 years	died, age 16 years	died, age 11 weeks	died, age 4 years	alive, age 0–1 year
	100% donor skin/gut GVHD marked infection- and drug-induced hyperresponsivity of the skin	100% donor fatal transplant- associated TMA	100% donor skin GVHD severe VOD long-term enteropathy liver cirrhosis ESRD (hemodialysis)	pneumonitis with capillary leak peri-engraftment GVHD skin and gut recurrence of VZV with fatal encephalopathy	100% donor skin GVHD (late) marked mucositis and skin toxicity adenoviraemia long-term enteropathy with norovirus infections	100% donor no GVHD episode of acute encephalopathy currently <3 months post-HSCT

ATG, antithymocyte globulin; Bu, busulfan; CADD, combined annotation dependent depletion; Cyclo, cyclophosphamide; ESRD, end-stage renal disease; Flu, fludarabine; GVHD, graft-versus-host disease; Mel, melphalan; MMF, mycophenolate mofetil; TREC, T cell receptor excision circles; Treo, treosulfan; URD, unrelated donor; VOD, veno-occlusive disease; VZV, varicella zoster virus.
[a]Allele frequency in GnomAD, dbSNP or ExAC databases.
[b]Parameters are presented with units and normal reference ranges if applicable.
[c]For this individual, TREC copies were available with significantly reduced levels.

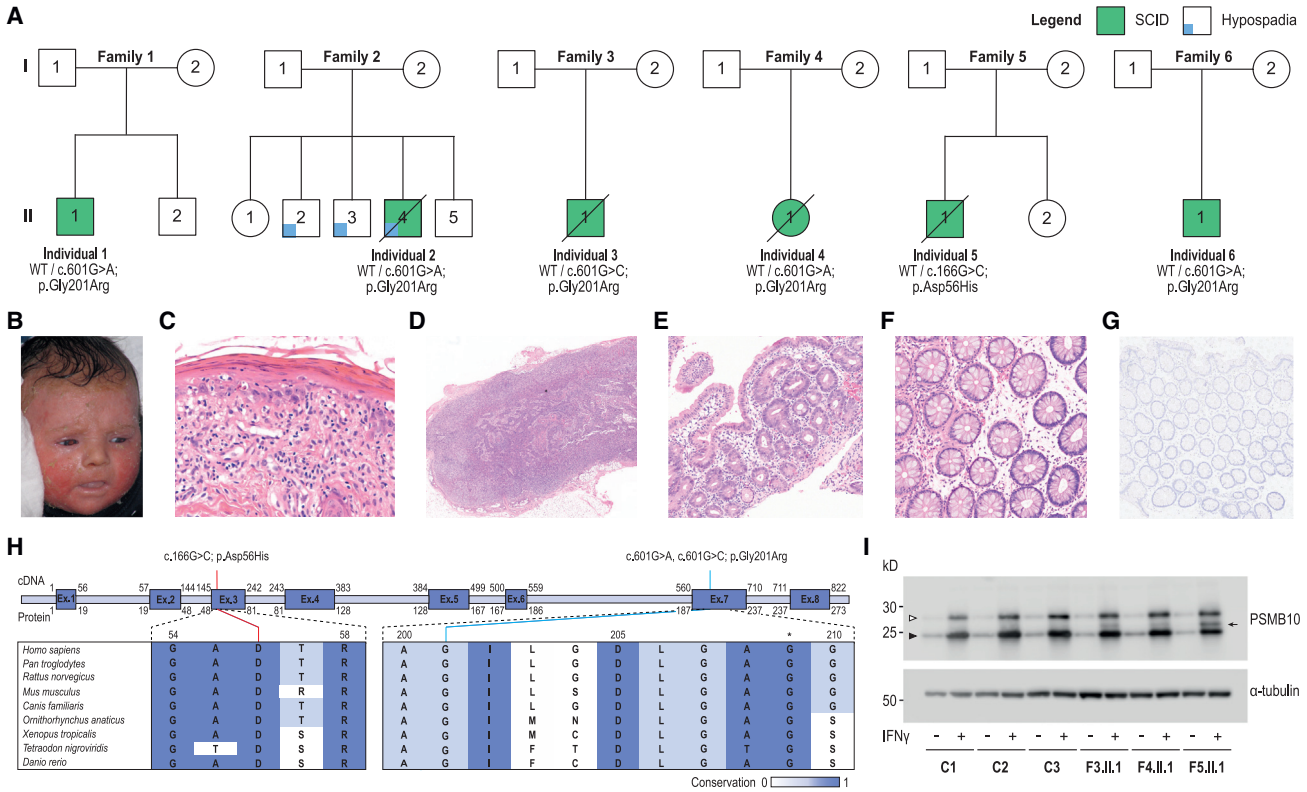

Figure 1. Clinical features and identification of *PSMB10 de novo* missense variants

(A) *PSMB10* variants in six infants with SCID.

(B) Erythematosquamous rash in individual 1 at 12 weeks after birth.

(C) Histology of the initial skin biopsy of individual 1 showed a graft-versus-host-disease-like pattern with vacuolar interface inflammation, multiple scattered apoptotic keratinocytes, and involvement of the adnexal structures, in the presence of a limited lymphocytic infiltrate (hematoxylin and eosin staining; original magnification ×41).

(D) Histopathological evaluation of an inguinal lymph node extracted from individual 5 showed a paucicellular, stroma-rich lymph node.

(E) A jejunal biopsy from individual 3 was hallmarked by partial villous atrophy and crypt hyperplasia with relatively few lymphocytes.

(F) Colonic mucosa biopsied from individual 5 showed preserved crypt architecture with an empty lamina propria with few lymphocytes, in keeping with an immunodeficiency-related enteropathy.

(G) Immunohistochemistry showed the absence of $CD3^+$ and $CD20^+$ positive cells in the colon samples from individual 5, although significant numbers of $CD4^+$ cells were observed that may be of a macrophage/monocyte lineage.

(H) Visualization of the three identified *PSMB10* variants at the cDNA and protein level. The conservation across species is shown and scaled by color. The asterisk indicates the position of a previously studied Psmb10 variant in TUB6 mice.

(I) Immunoblot for PSMB10 in dermal fibroblasts of 3 controls, individual 3 (F3.II.1; p.Gly201Arg), individual 4 (F4.II.1; p.Gly201Arg), and individual 5 (F5.II.1; p.Asp56His), with or without prior IFN-gamma induction. Upper band (white arrowhead) represents immature and lower band (black arrowhead), mature, PSMB10; subject samples also show an additional, intermediate band (black arrow). Representative of 4 independent experiments.

(although not pathognomonic of) dominant-negative behavior.

Moreover, a genome-wide single-nucleotide polymorphism (SNP) microarray in individual 1, performed on blood-derived DNA before transplant at the age of 2 months, identified a partial somatic uniparental disomy (UPD) of chromosome 16 (UPD16) overlapping the *PSMB10* locus, indicating an aberrant B-allele frequency (BAF) profile on the q arm of chromosome 16 spanning ~24 Mb from 16q21 to the terminal end of 16q (16qter) (Figure 2A). Further validation in buccal tissue at the age of 8 and 13 years demonstrated a different UPD, roughly ~10 Mb more proximal (16q12.1) (Figure 2A). The two independent UPDs presumably originated during mitotic recombination where in a single progenitor cell, the germline mutation was restored with a wild-type copy of the unaffected parental chromosome. Ultra-deep amplicon sequencing demonstrated a slightly higher rate of RM in blood, with respective variant allele frequencies (VAFs) of 39.98% for blood-derived DNA obtained before transplant and 42.90% for buccal-swab DNA collected at age 13, suggesting that 79.96% and 85.80% of cells are heterozygous for the *PSMB10* mutation (Figure 2B). We cannot exclude the fact that this slight difference might be due to contamination of buccal swab DNA with post-HSCT wild-type blood-derived DNA. Subsequently, we have adapted our haplarithmisis method for trio WES data to confirm the somatic UPD and to determine its parental origin. The level

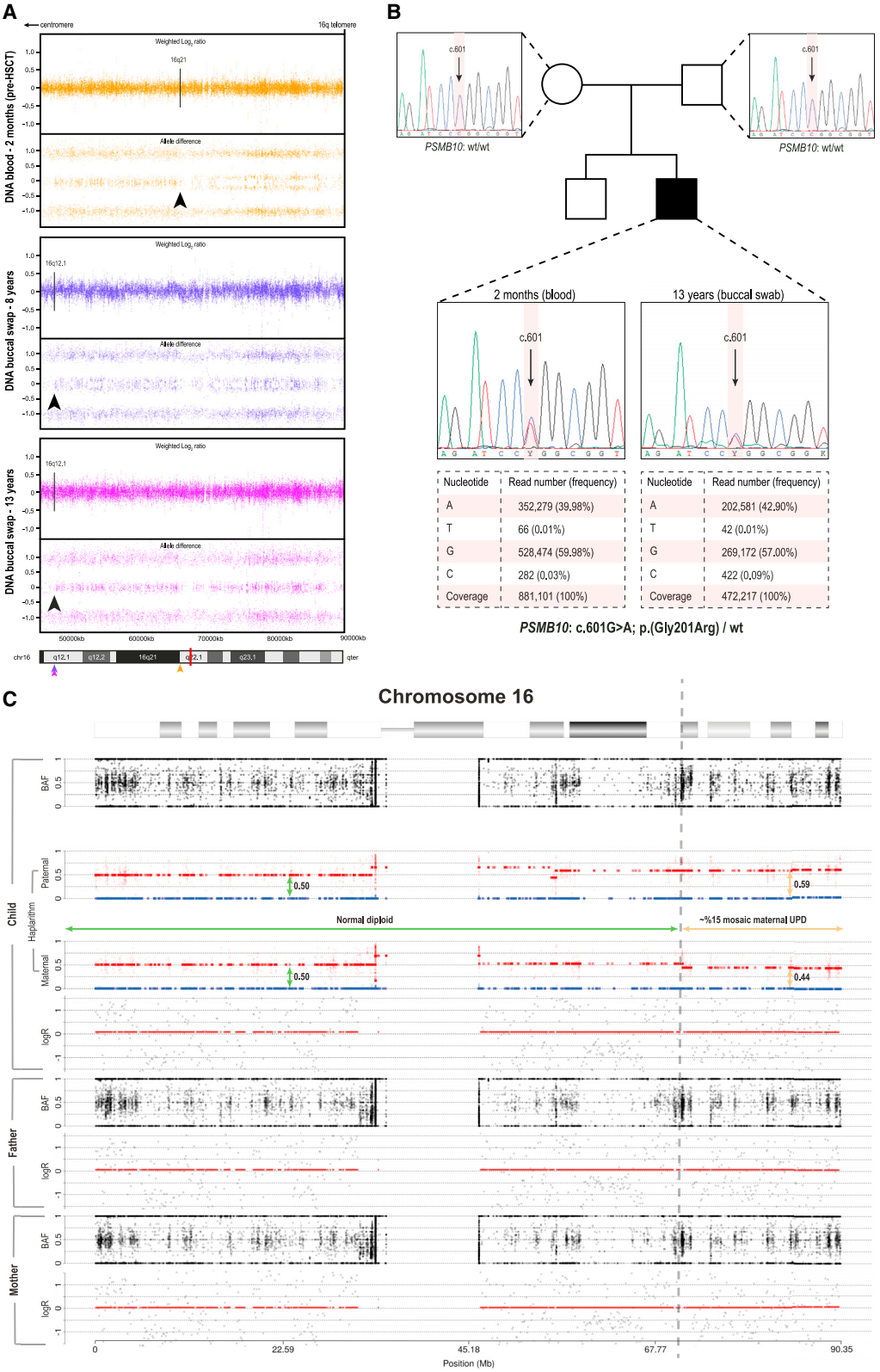

Figure 2. Acquired segmental UPD overlapping the PSMB10 locus shows evidence of RM

(A) Aberrant BAF profile of the genome-wide SNP-array analysis in individual 1 reveals two independent UPD events at the q arm of chromosome 16 in blood (pre-HSCT at 2 months of age; 16q12.1) and in the buccal mucosa (16q12.1) spanning to the terminal end of 16q (16qter). Arrows indicate the respective breakpoints of UPD and are color-coded for each tissue; the red bar in the ideogram represents the distinct location of *PSMB10*.

(legend continued on next page)

of mosaicism was estimated by calculating the distortion of segmented haplarithm values from the expected 1:1 allelic ratio, i.e., 0.5:0.5 vertical distance in each segmented parental haplarithm. This approach confirmed that the p arm of chromosome 16 shows both parental haplotypes present in 0.5:0.5 vertical distance (green vertical arrows), but also suggests a somatic UPD by RM in blood-derived DNA, resulting in a paternal allele bias of 0.59 (9% distortion from BAF, upper orange vertical bar) and maternal allele bias of 0.44 (6% distortion from BAF, lower orange vertical bar), resulting in a 15% mosaic maternal UPD on chromosome 16q21–qter (Figure 2C). The proportion of cells that were estimated to be restored to wild-type following the 15% maternal UPD event correlated with the 20% of cells that were homozygous wild-type based on amplicon sequencing data. There was no indication of the presence of RM in the other individuals.

Next, we modeled the structural impact of both missense variants using experimentally determined 3D structures of PSMB10 and the 20S proteasome (Figure 3A). Both the aspartic acid at position 56 and the glycine at position 201 hold highly conserved positions in β2i/PSMB10 and are positioned at the β-ring interface in close proximity to residues in regulating domains that facilitate incorporation into the proteasome 20S complex through interaction with surrounding subunits (Figure 3B). Substitutions of the acidic aspartic acid to the larger, basic histidine and the highly flexible wild-type glycine for the substantially larger mutant arginine are expected to cause significant disruption to the local structural environment due to the inability to fit within the same spatial constraints (Figure 3B). In particular, the β-ring/β-ring interaction between β2i and β7 (PSMB4) is predicted to be affected by steric clashes, leading to misfolding of the β2i subunit. This is supported by energy calculations of protein stability, indicating that the variants induce a high change in Gibbs free energy (ΔΔG) and are thus highly destabilizing for the 20S IP structure (Figures 3C–3F).

Subsequently, we compared the effect of the p.Gly201Arg variant to a published TUB6 mouse model harboring the ENU (N-ethyl-N-nitrosourea) mutagenesis-generated c.625G>T (p.Gly209Trp) variant in Psmb10 (reported as p.Gly170Trp based on sequence alignment to *Thermoplasma acidophilum*), causing a phenotype reminiscent of human OS and sterile autoinflammation.[30–33] When superposing the structures of the human and mouse PSMB10 and 20S IP, we observed a high degree of structural similarity (Figure 4A). Structural alignment showed that both glycine variants were in close proximity (Figure 4B). We noted that p.Gly209Trp conferred similar destabilizing effects as p.Gly201Arg, owing to the bulky nature of tryptophan amino acid at position 209 that introduces steric clashes with the neighboring residues (Figure 4C). The variant was predicted to have a more destabilizing impact on 20S IP structure as compared to the human variants (Figure 4D). Moreover, the p.Asp56His and p.Gly201Arg variants were predicted to be slightly less destabilizing for the full 26S proteasome as compared to the 20S IP (Figure 4D).

The clinical and immunological phenotypes of the individuals we studied contrast with classical PRAAS (Table 1) and instead fulfills diagnostic criteria for SCID-OS syndrome.[27] Infants presented early with FTT, erythroderma, diarrhea, oral candidiasis, opportunistic infections, and inflammatory phenomena involving the skin and GI tract. Consistent with OS, they had a reduced number and function of T and B lymphocytes, hypereosinophilia, variability in NK lymphocyte numbers, T cell clonal expansion, and impaired T cell proliferation. Histological features in skin were compatible with OS without PRAAS-characteristic signs of neonatal-onset neutrophilic dermatosis or lipoatrophy.[11] B cell maturation in the BM was severely reduced in a pattern similar to that seen in classical OS caused by defects of V(D)J recombination (Figure S1). Compared to OS, an important difference is the poor HSCT outcome in our studied individuals, with higher incidence of GVHD and mortality.[34,35] In particular, the chronic enteropathy and skin hypersensitivity remaining post-GVHD in these tissues were remarkable. Previously, persons with PRAAS due to POMP deficiency and recessive mutations in *PSMB4* have successfully undergone HSCT without severe post-transplant complications.[17,18,36,37] Although potential benefit of treatment with JAK inhibitors has been demonstrated in individuals with type I interferonopathies, including PRAAS, the role of dysregulated type I IFN signaling in individuals with (severe) combined immunodeficiency due to proteasome-associated mutations remains to be elucidated.[13,38]

Autosomal-recessive mutations in *PSMB10* have been described in individuals with PRAAS without immunodeficiency.[11,19] All four reported individuals carried compound heterozygous or homozygous mutations affecting the phenylalanine residue at position 14, located in the N-terminal pro-peptide sequence. These mutations interfered with cleavage of PSMB10, thereby impairing β2i maturation, proteasome assembly, and trypsin-like catalytic function.[11,19] In contrast, the clinical features of our studied individuals, with in part recurrent *de novo* mutations, recall

(B) Exome inclusion of the unaffected parents of individual 1 resulted in the identification of a unique heterozygous *de novo* missense mutation in *PSMB10* (c.601G>A [GenBank: NM_002801.3] [p.Gly201Arg]). *De novo* status was verified by Sanger sequencing, while deep amplicon sequencing using the Ion Torrent accurately determined the respective mosaic levels in both tissues.
(C) Results from haplarithmisis on blood-derived DNA from individual 1 (pre-HSCT at 2 months of age) and parents. From top to bottom we depict BAF, paternal haplarithm, maternal haplarithm, and logR (relative copy number) values of the child, followed by BAF and logR-values of the parents. BAF of a single-nucleotide variant (SNV) is the number of allele B over the number of alleles A and B for that SNV, and logR is the base 2 logarithm of the summed normalized number of both alleles in a window of 100 kb over the expected signal intensity values.

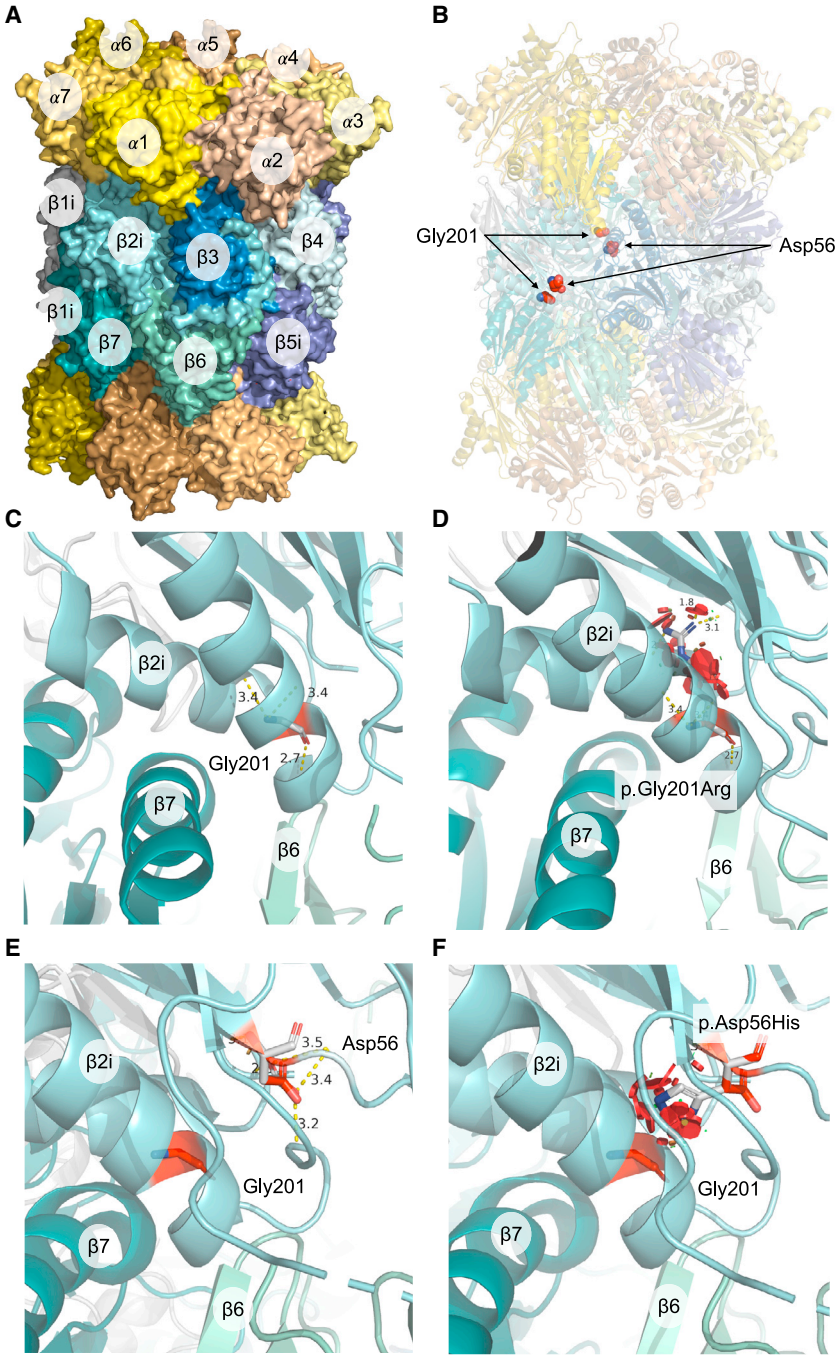

Figure 3. Predicted structural consequences of the *PSMB10* variants

(A) Crystal structure of human IP 20S particle (PDB: 6E5B) is shown with its alpha subunits in shades of yellow/orange and beta subunits in shades of blue/green.

(B) Positions of interest, Gly201 and Asp56, in the β2i subunits are highlighted as red spheres. The local structural environment of Gly201 (sticks) is depicted in (C) including distances from its interacting residues in the α-helix, which is located close to the β-ring interface.

(D) Local structural clashes (in red discs) potentially brought about by p.Gly201Arg are shown. Together with the drastic changes in free energy of the complex, p.Gly201Arg appears to be structurally damaging. Similar structural representations are illustrated for the variant p.Asp56His in (E) and (F), which also include the position Gly201 for visual reference.

the recent description of two immunodeficient children with *de novo* missense mutation in *PSMB9*, which the authors termed PRAAS with immunodeficiency (PRAAS-ID) to distinguish it from the classic PRAAS phenotype.[13] Shared features with our *PSMB10*-mutated infants included infections and chronic viremia, liver dysfunction, skin rash, absence of lipoatrophy and a combined T and B cell defect with an increased CD4/CD8 ratio, skewing toward a CD8 T cell memory phenotype, and hypogammaglobulinemia. The authors demonstrated that the c.494G>A (p.Gly156Asp) substitution impaired maturation of the PSMB9/β1i, β2i, and β5i subunits and abrogated activity of the 20S but not the 26S IP.[13,39] The clinical and functional phenotype was recapitulated in mice that had a knockin of the identified p.Gly156Asp variant, except for the autoinflammatory symptoms including fever and myositis.[13] *In silico* structure modeling indicated that the p.Gly156Asp variant disturbed the β-ring/β-ring interaction without affecting the active site conformation. Similar variant effects were predicted for our *PSMB10* mutations. Given the co-dependent incorporation of the β1i and β2i subunits that together facilitate β5i incorporation, overall misfolding of all three βi-subunits was predicted, rather than a selective impact on β2i's enzymatic (trypsin-like) activity.[4] Since the IP incorporates two of each subunit into the catalytic core, we hypothesize that the p.Asp56His and p.Gly201Arg PSMB10 variants would exert similar dominant-negative effects.

The observed p.Gly201Arg substitution is located in close proximity to the *Psmb10* p.Gly209Trp variant in TUB6 mice.[30] Homozygous mice presented with T-B-NK-SCID, sterile autoinflammation, hyperkeratosis of the skin, alopecia, neutrophilic infiltration, lipoatrophy, and a reduced life span, while heterozygous mice exhibited an isolated T cell defect with decreased T cell number, elevated CD4/CD8 ratio, and susceptibility to *Listeria* infection.[30] The overlap of these features in mice compared with our studied individuals is striking, although the heterozygous mice exhibited less severe features, likely due to a more robust compensation of

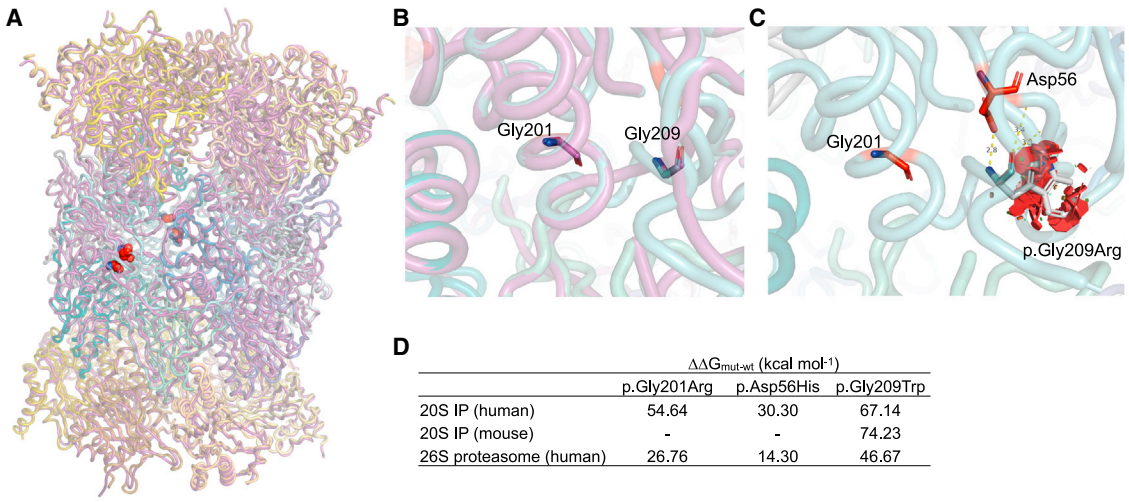

D

	$\Delta\Delta G_{mut\text{-}wt}$ (kcal mol^{-1})		
	p.Gly201Arg	p.Asp56His	p.Gly209Trp
20S IP (human)	54.64	30.30	67.14
20S IP (mouse)	-	-	74.23
26S proteasome (human)	26.76	14.30	46.67

Figure 4. Comparison of predicted structural impact of variants on human and mouse PSMB10
(A) Superposition of human (PDB: 6E5B) and mouse (PDB: 3UNH, purple) 20S IP crystal structures is shown (root-mean-square deviation [RMSD] = 0.59 Å), with the positions of interest highlighted in red spheres. The local structural environment of Gly201 and Gly209 is depicted in (B), which highlights the clear overlap of residues between human (cyan) and mouse (purple) PSMB10.
(C) The steric clashes potentially brought about by Gly209 in human 20S IP are illustrated as red discs, suggesting a structurally damaging outcome of the p.Gly209Trp variant. The table in (D) lists the predicted differences in free energies of the proteasome complexes for each variant type for each protein system.

heterozygous mutations generally observed in mice. Although mice did show neutrophilic infiltration and lipoatrophy at 8 weeks, the apparent lack of autoinflammatory symptoms in affected children could be due to the early intervention with HSCT. Interestingly, individual 2 displayed hemophagocytic lymphohistiocytosis (HLH)-like inflammation and was transplanted last at the age of 2.5 years. In addition, the severe post-HSCT inflammatory complications might be related to the underlying IP defect, perhaps resulting from an impaired function in extra-hematopoietic tissues such as in the epithelial cells of the skin and gut. Furthermore, the p.Gly209Trp Psmb10 variant was predicted to disrupt β-ring/β-ring interaction similar to p.Gly201Arg and was expected to dramatically impact 20S IP complex formation and, to a lesser extent, the 26S proteasome. Since β2i is incorporated into the thymoproteasome along with β1i and β5t, and TUB6 mice lacked cortical thymic epithelial cells that are important for T cell development, thymic dysfunction might contribute to the observed T cell phenotype in our individuals.[40] In addition, dominant-negative missense mutations are hypothesized to prevent substitution of the mutated subunits by their constitutive counterparts and affect the stability of core 20S proteasome that interferes with homeostatic IP functions beyond CD8 T cell function and MHC-I antigen presentation as observed in single, double, or triple PSMB8/β5i, PSMB9/β1i and PSMB10/β2i knockout mouse models.[3,41–43] These include removal of unfolded and oxidized proteins and T cell proliferation, differentiation and survival independent of MHC-I antigen presentation capabilities, especially in the context of inflammation.[44–46] Therefore, the observed defects in T and B cell development and maturation in our individuals might suggest a mutation-specific defect in these homeostatic functions cumulating in proteotoxic stress.[47] In addition, PSMB10 might have a direct role in V(D)J recombination.

This study also demonstrates that the evaluation of RM in trio-based exome data using the haplarithmisis method offers a unique, sensitive mapping strategy that, depending on the quality of UPD mapping and the detection sensitivity, has the potential to trace previously undetected mutations. RM delineates the rare phenomenon in which the occurrence and/or accumulation of spontaneous somatic mutations coincides with the direct or indirect rescue of a pathogenic germline mutation,[48] in essence suggesting natural evidence for the repair of a functional defect caused by the *de novo* mutation in *PSMB10*. RM has been observed to have a beneficial clinical impact for a range of IEI, including OS.[49–51] The co-occurrence of a *de novo PSMB10* mutation with RM is unlikely to be a chance finding, demonstrates an elegant but possibly underestimated disease gene mapping strategy, and is suggestive for a strong cellular effect of the respective *PSMB10* mutation and an associated evolutionary pressure of mutated cell lineages.[48] To our knowledge, exome data have not been used to detect and visualize haplotype revertant mosaics, and we propose that this approach should be applied more often to individuals with IEI as a mapping strategy for disease gene identification. It is intriguing that the only person to achieve full T cell reconstitution post-transplant also demonstrated partial somatic reversion of the *PSMB10* mutation.

In summary, our study reports *de novo* autosomal-dominant, suspected dominant-negative, *PSMB10* missense mutations as a cause of SCID-OS (PSMB10-OS) that should be

sought in NBS. Furthermore, these findings expand the spectrum of proteasome-associated monogenic diseases.

Data and code availability

The article includes all datasets generated or analyzed during this study. The exome-sequencing data of the five families supporting the current study have not been deposited in a public repository because of privacy issues but are available from the corresponding author on request.

Supplemental information

Supplemental information can be found online at https://doi.org/10.1016/j.ajhg.2024.02.013.

Acknowledgments

We would like to thank the individuals and their families for participation in this study. We acknowledge colleagues from our diagnostic division (Genome Diagnostics Nijmegen), the Radboud Genomics Technology Center, and all members of the Radboud University Medical Center multidisciplinary immune-disease board and colleagues at Great North Children's Hospital, Great Ormond St Hospital for Children, and sister hospitals. C.I.v.d.M., S.K., and A.H. were supported by the Radboud Institute for Molecular Life Sciences. G.R. was supported by the Europees Fonds voor Regionale Ontwikkeling (EFRO) (R0005582). T.M. was supported by the Sigrid Jusélius Foundation. M.G.N. was supported by the Nederlandse Organisatie voor Wetenschappelijk Onderzoek (Spinoza grant) and the European Research Council (grant agreement no. 310372). F.L.v.d.V. was supported by a ZonMW Vidi grant. R.S. is supported by the Israel Science Foundation (ISF) under the Israel Precision Medicine Program (IPMP), grant agreement no. 3115/19. S.H. was supported by the Wellcome Trust (grant number 207556_Z_17_Z). A.H. was supported by the Solve-RD project, which has received funding from the European Union's Horizon 2020 research and innovation programme under grant agreement no. 779257.

Author contributions

Conceptualization: C.I.v.d.M., S.K., O.C., R.S., S.H., S.S.V.H., and A.H.; data curation: C.I.v.d.M., S.K., O.C., K.R.E., G.R., H.G., and I.S.v.d.L.; formal analysis: C.I.v.d.M., S.K., G.R., H.V., R.E., and M.Z.E.; funding acquisition: M.G.N., F.L.v.d.V., R.S., S.H., A.H.; investigation: C.I.v.d.M., S.K., O.C., K.R.E., G.R., H.G., I.S.v.d.L., H.V., R.S., M.Z.E., M.v.d.B., and S.H.; resources: A.R.R., M.S., J.H.M.S., T.M., M.Z.E., A.L.A., P.S.L., A.S., R.P., A.W., M.M.S., M.A.S., T.F., A.R.G., A.J.S., A.L., S.F., O.B., M.v.d.B., R.S., S.H., and A.H.; supervision: F.L.v.d.V., M.G.N., R.S., S.H., S.S.V.H., and A.H.; visualization: C.I.v.d.M., S.K., G.R., R.E., and M.Z.E.; writing – original draft: C.I.v.d.M. and S.K.; writing – review and editing: all authors. All authors read and approve the final manuscript.

Declaration of interests

The authors declare no competing interests.

Received: October 5, 2023
Accepted: February 22, 2024
Published: March 18, 2024

References

1. Murata, S., Takahama, Y., Kasahara, M., and Tanaka, K. (2018). The immunoproteasome and thymoproteasome: functions, evolution and human disease. Nat. Immunol. *19*, 923–931. https://doi.org/10.1038/s41590-018-0186-z.
2. McCarthy, M.K., and Weinberg, J.B. (2015). The immunoproteasome and viral infection: a complex regulator of inflammation. Front. Microbiol. *6*, 21. https://doi.org/10.3389/fmicb.2015.00021.
3. Kincaid, E.Z., Che, J.W., York, I., Escobar, H., Reyes-Vargas, E., Delgado, J.C., Welsh, R.M., Karow, M.L., Murphy, A.J., Valenzuela, D.M., et al. (2011). Mice completely lacking immunoproteasomes show major changes in antigen presentation. Nat. Immunol. *13*, 129–135. https://doi.org/10.1038/ni.2203.
4. Van den Eynde, B.J., and Morel, S. (2001). Differential processing of class-I-restricted epitopes by the standard proteasome and the immunoproteasome. Curr. Opin. Immunol. *13*, 147–153. https://doi.org/10.1016/S0952-7915(00)00197-7.
5. Heink, S., Ludwig, D., Kloetzel, P.-M., and Krüger, E. (2005). IFN-γ-induced immune adaptation of the proteasome system is an accelerated and transient response*102*, pp. 9241–9246. https://doi.org/10.1073/pnas.0501711102.
6. Nitta, T., Murata, S., Sasaki, K., Fujii, H., Ripen, A.M., Ishimaru, N., Koyasu, S., Tanaka, K., and Takahama, Y. (2010). Thymoproteasome Shapes Immunocompetent Repertoire of CD8+ T Cells. Immunity *32*, 29–40. https://doi.org/10.1016/j.immuni.2009.10.009.
7. Arima, K., Kinoshita, A., Mishima, H., Kanazawa, N., Kaneko, T., Mizushima, T., Ichinose, K., Nakamura, H., Tsujino, A., Kawakami, A., et al. (2011). Proteasome assembly defect due to a proteasome subunit beta type 8 (PSMB8) mutation causes the autoinflammatory disorder, Nakajo-Nishimura syndrome*108*, pp. 14914–14919. https://doi.org/10.1073/pnas.1106015108.
8. Brehm, A., Liu, Y., Sheikh, A., Marrero, B., Omoyinmi, E., Zhou, Q., Montealegre, G., Biancotto, A., Reinhardt, A., Almeida De Jesus, A., et al. (2015). Additive loss-of-function proteasome subunit mutations in CANDLE/PRAAS patients promote type I IFN production. J. Clin. Invest. *125*, 4196–4211. https://doi.org/10.1172/JCI81260.
9. De Jesus, A.A., Brehm, A., VanTries, R., Pillet, P., Parentelli, A.-S., Montealegre Sanchez, G.A., Deng, Z., Paut, I.K., Goldbach-Mansky, R., and Krüger, E. (2019). Novel proteasome assembly chaperone mutations in PSMG2/PAC2 cause the autoinflammatory interferonopathy CANDLE/PRAAS4. J. Allergy Clin. Immunol. *143*, 1939–1943.e8. https://doi.org/10.1016/j.jaci.2018.12.1012.
10. Kitamura, A., Maekawa, Y., Uehara, H., Izumi, K., Kawachi, I., Nishizawa, M., Toyoshima, Y., Takahashi, H., Standley, D.M., Tanaka, K., et al. (2011). A mutation in the immunoproteasome subunit PSMB8 causes autoinflammation and lipodystrophy in humans. J. Clin. Invest. *121*, 4150–4160. https://doi.org/10.1172/JCI58414.
11. Papendorf, J.J., Ebstein, F., Alehashemi, S., Piotto, D.G.P., Kozlova, A., Terreri, M.T., Shcherbina, A., Rastegar, A., Rodrigues, M., Pereira, R., et al. (2023). Identification of eight novel proteasome variants in five unrelated cases of proteasome-associated

autoinflammatory syndromes (PRAAS). Front. Immunol. *14*, 1190104.

12. Poli, M.C., Ebstein, F., Nicholas, S.K., de Guzman, M.M., Forbes, L.R., Chinn, I.K., Mace, E.M., Vogel, T.P., Carisey, A.F., Benavides, F., et al. (2018). Heterozygous Truncating Variants in POMP Escape Nonsense-Mediated Decay and Cause a Unique Immune Dysregulatory Syndrome. Am. J. Hum. Genet. *102*, 1126–1142. https://doi.org/10.1016/j.ajhg.2018.04.010.
13. Kanazawa, N., Hemmi, H., Kinjo, N., Ohnishi, H., Hamazaki, J., Mishima, H., Kinoshita, A., Mizushima, T., Hamada, S., Hamada, K., et al. (2021). Heterozygous missense variant of the proteasome subunit β-type 9 causes neonatal-onset autoinflammation and immunodeficiency. Nat. Commun. *12*, 6819. https://doi.org/10.1038/s41467-021-27085-y.
14. Agarwal, A.K., Xing, C., DeMartino, G.N., Mizrachi, D., Hernandez, M.D., Sousa, A.B., Martínez de Villarreal, L., Dos Santos, H.G., and Garg, A. (2010). PSMB8 Encoding the β5i Proteasome Subunit Is Mutated in Joint Contractures, Muscle Atrophy, Microcytic Anemia, and Panniculitis-Induced Lipodystrophy Syndrome. Am. J. Hum. Genet. *87*, 866–872. https://doi.org/10.1016/j.ajhg.2010.10.031.
15. Garg, A., Hernandez, M.D., Sousa, A.B., Subramanyam, L., Martínez de Villarreal, L., dos Santos, H.G., and Barboza, O. (2010). An Autosomal Recessive Syndrome of Joint Contractures, Muscular Atrophy, Microcytic Anemia, and Panniculitis-Associated Lipodystrophy. J. Clin. Endocrinol. Metab. *95*, E58–E63. https://doi.org/10.1210/jc.2010-0488.
16. Liu, Y., Ramot, Y., Torrelo, A., Paller, A.S., Si, N., Babay, S., Kim, P.W., Sheikh, A., Lee, C.C.R., Chen, Y., et al. (2012). Mutations in proteasome subunit β type 8 cause chronic atypical neutrophilic dermatosis with lipodystrophy and elevated temperature with evidence of genetic and phenotypic heterogeneity. Arthritis Rheum. *64*, 895–907. https://doi.org/10.1002/art.33368.
17. Gatz, S.A., Salles, D., Jacobsen, E.-M., Dörk, T., Rausch, T., Aydin, S., Surowy, H., Volcic, M., Vogel, W., Debatin, K.-M., et al. (2016). MCM3AP and POMP Mutations Cause a DNA-Repair and DNA-Damage-Signaling Defect in an Immunodeficient Child. Hum. Mutat. *37*, 257–268. https://doi.org/10.1002/humu.22939.
18. Verhoeven, D., Schonenberg-Meinema, D., Ebstein, F., Papendorf, J.J., Baars, P.A., van Leeuwen, E.M.M., Jansen, M.H., Lankester, A.C., van der Burg, M., Florquin, S., et al. (2022). Hematopoietic stem cell transplantation in a patient with proteasome-associated autoinflammatory syndrome (PRAAS). J. Allergy Clin. Immunol. *149*, 1120–1127.e8. https://doi.org/10.1016/j.jaci.2021.07.039.
19. Sarrabay, G., Méchin, D., Salhi, A., Boursier, G., Rittore, C., Crow, Y., Rice, G., Tran, T.-A., Cezar, R., Duffy, D., et al. (2020). PSMB10, the last immunoproteasome gene missing for PRAAS. J. Allergy Clin. Immunol. *145*, 1015–1017.e6. https://doi.org/10.1016/j.jaci.2019.11.024.
20. Ansar, M., Ebstein, F., Özkoç, H., Paracha, S.A., Iwaszkiewicz, J., Gesemann, M., Zoete, V., Ranza, E., Santoni, F.A., Sarwar, M.T., et al. (2020). Biallelic variants in PSMB1 encoding the proteasome subunit β6 cause impairment of proteasome function, microcephaly, intellectual disability, developmental delay and short stature. Hum. Mol. Genet. *29*, 1132–1143. https://doi.org/10.1093/hmg/ddaa032.
21. Küry, S., Besnard, T., Ebstein, F., Khan, T.N., Gambin, T., Douglas, J., Bacino, C.A., Craigen, W.J., Sanders, S.J., Lehmann, A., et al. (2017). De Novo Disruption of the Proteasome Regulatory Subunit PSMD12 Causes a Syndromic Neurodevelopmental Disorder. Am. J. Hum. Genet. *100*, 352–363. https://doi.org/10.1016/j.ajhg.2017.01.003.
22. Yan, K., Zhang, J., Lee, P.Y., Tao, P., Wang, J., Wang, S., Zhou, Q., and Dong, M. (2022). Haploinsufficiency of PSMD12 Causes Proteasome Dysfunction and Subclinical Autoinflammation. Arthritis Rheumatol. *74*, 1083–1090. https://doi.org/10.1002/art.42070.
23. Mégarbané, A., Sanders, A., Chouery, E., Delague, V., Medlej-Hashim, M., and Torbey, P.-H. (2002). An unknown autoinflammatory syndrome associated with short stature and dysmorphic features in a young boy. J. Rheumatol. *29*, 1084–1087.
24. Khalil, R., Kenny, C., Hill, R.S., Mochida, G.H., Nasir, R., Partlow, J.N., Barry, B.J., Al-Saffar, M., Egan, C., Stevens, C.R., et al. (2018). *PSMD12* haploinsufficiency in a neurodevelopmental disorder with autistic features. American J of Med Genetics Pt B *177*, 736–745. https://doi.org/10.1002/ajmg.b.32688.
25. Ebstein, F., Küry, S., Rosenfelt, C., Scott-Boyer, M., van Woerden, M., Besnard, T., Papendorf, J.J., Studencka-Turski, M., Wang, T., Hsieh, T., et al. (2023). PSMC3 proteasome subunit variants are associated with neurodevelopmental delay and type I interferon production. Sci.Transl.Med. *15*, eabo3189. https://doi.org/10.1126/scitranslmed.abo3189.
26. Kröll-Hermi, A., Ebstein, F., Stoetzel, C., Geoffroy, V., Schaefer, E., Scheidecker, S., Bär, S., Takamiya, M., Kawakami, K., Zieba, B.A., et al. (2020). Proteasome subunit *PSMC3* variants cause neurosensory syndrome combining deafness and cataract due to proteotoxic stress. EMBO Mol. Med. *12*, e11861. https://doi.org/10.15252/emmm.201911861.
27. Dvorak, C.C., Haddad, E., Heimall, J., Dunn, E., Cowan, M.J., Pai, S.-Y., Kapoor, N., Satter, L.F., Buckley, R.H., O'Reilly, R.J., et al. (2023). The diagnosis of severe combined immunodeficiency: Implementation of the PIDTC 2022 Definitions. J. Allergy Clin. Immunol. *151*, 547–555.e5. https://doi.org/10.1016/j.jaci.2022.10.021.
28. Hebert, A., Simons, A., Schuurs-Hoeijmakers, J.H.M., Koenen, H.J.P.M., Zonneveld-Huijssoon, E., Henriet, S.S.V., Schatorjé, E.J.H., Hoppenreijs, E.P.A.H., Leenders, E.K.S.M., Janssen, E.J.M., et al. (2022). Trio-based whole exome sequencing in patients with suspected sporadic inborn errors of immunity: a retrospective cohort study. Elife *11*, e78469. https://doi.org/10.7554/eLife.78469.
29. Tangye, S.G., Al-Herz, W., Bousfiha, A., Cunningham-Rundles, C., Franco, J.L., Holland, S.M., Klein, C., Morio, T., Oksenhendler, E., Picard, C., et al. (2022). Human Inborn Errors of Immunity: 2022 Update on the Classification from the International Union of Immunological Societies Expert Committee. J. Clin. Immunol. *42*, 1473–1507. https://doi.org/10.1007/s10875-022-01289-3.
30. Treise, I., Huber, E.M., Klein-Rodewald, T., Heinemeyer, W., Grassmann, S.A., Basler, M., Adler, T., Rathkolb, B., Helming, L., Andres, C., et al. (2018). Defective immuno- and thymoproteasome assembly causes severe immunodeficiency. Sci. Rep. *8*, 5975. https://doi.org/10.1038/s41598-018-24199-0.
31. Zamani Esteki, M., Viltrop, T., Tšuiko, O., Tiirats, A., Koel, M., Nõukas, M., Žilina, O., Teearu, K., Marjonen, H., Kahila, H., et al. (2019). In vitro fertilization does not increase the incidence of de novo copy number alterations in fetal and placental lineages. Nat. Med. *25*, 1699–1705. https://doi.org/10.1038/s41591-019-0620-2.

32. Zamani Esteki, M., Dimitriadou, E., Mateiu, L., Melotte, C., Van der Aa, N., Kumar, P., Das, R., Theunis, K., Cheng, J., Legius, E., et al. (2015). Concurrent Whole-Genome Haplotyping and Copy-Number Profiling of Single Cells. Am. J. Hum. Genet. *96*, 894–912. https://doi.org/10.1016/j.ajhg.2015.04.011.
33. Essers, R., Lebedev, I.N., Kurg, A., Fonova, E.A., Stevens, S.J.C., Koeck, R.M., Von Rango, U., Brandts, L., Deligiannis, S.P., Nikitina, T.V., et al. (2023). Prevalence of chromosomal alterations in first-trimester spontaneous pregnancy loss. Nat. Med. *29*, 3233–3242. https://doi.org/10.1038/s41591-023-02645-5.
34. Mazzolari, E., Moshous, D., Forino, C., De Martiis, D., Offer, C., Lanfranchi, A., Giliani, S., Imberti, L., Pasic, S., Ugazio, A.G., et al. (2005). Hematopoietic stem cell transplantation in Omenn syndrome: a single-center experience. Bone Marrow Transplant. *36*, 107–114. https://doi.org/10.1038/sj.bmt.1705017.
35. Schuetz, C., Gerke, J., Ege, M., Walter, J., Kusters, M., Worth, A., Kanakry, J.A., Dimitrova, D., Wolska-Kuśnierz, B., Chen, K., et al. (2023). Hypomorphic RAG deficiency: impact of disease burden on survival and thymic recovery argues for early diagnosis and HSCT. Blood *141*, 713–724. https://doi.org/10.1182/blood.2022017667.
36. Martinez, C., Ebstein, F., Nicholas, S.K., De Guzman, M., Forbes, L.R., Delmonte, O.M., Bosticardo, M., Castagnoli, R., Krance, R., Notarangelo, L.D., et al. (2021). HSCT corrects primary immunodeficiency and immune dysregulation in patients with POMP-related autoinflammatory disease. Blood *138*, 1896–1901. https://doi.org/10.1182/blood.2021011005.
37. Meinhardt, A., Ramos, P.C., Dohmen, R.J., Lucas, N., Lee-Kirsch, M.A., Becker, B., De Laffolie, J., Cunha, T., Niehues, T., Salzer, U., et al. (2021). Curative Treatment of POMP-Related Autoinflammation and Immune Dysregulation (PRAID) by Hematopoietic Stem Cell Transplantation. J. Clin. Immunol. *41*, 1664–1667. https://doi.org/10.1007/s10875-021-01067-7.
38. Sanchez, G.A.M., Reinhardt, A., Ramsey, S., Wittkowski, H., Hashkes, P.J., Berkun, Y., Schalm, S., Murias, S., Dare, J.A., Brown, D., et al. (2018). JAK1/2 inhibition with baricitinib in the treatment of autoinflammatory interferonopathies. J. Clin. Invest. *128*, 3041–3052. https://doi.org/10.1172/JCI98814.
39. Kataoka, S., Kawashima, N., Okuno, Y., Muramatsu, H., Miwata, S., Narita, K., Hamada, M., Murakami, N., Taniguchi, R., Ichikawa, D., et al. (2021). Successful treatment of a novel type I interferonopathy due to a de novo PSMB9 gene mutation with a Janus kinase inhibitor. J. Allergy Clin. Immunol. *148*, 639–644. https://doi.org/10.1016/j.jaci.2021.03.010.
40. Murata, S., Sasaki, K., Kishimoto, T., Niwa, S.I., Hayashi, H., Takahama, Y., and Tanaka, K. (2007). Regulation of $CD8^+$ T Cell Development by Thymus-Specific Proteasomes. Science *316*, 1349–1353. https://doi.org/10.1126/science.1141915.
41. Fehling, H.J., Swat, W., Laplace, C., Kühn, R., Rajewsky, K., Müller, U., and Von Boehmer, H. (1994). MHC Class I Expression in Mice Lacking the Proteasome Subunit LMP-7. Science *265*, 1234–1237. https://doi.org/10.1126/science.8066463.
42. Van Kaer, L., Ashton-Rickardt, P.G., Eichelberger, M., Gaczynska, M., Nagashima, K., Rock, K.L., Goldberg, A.L., Doherty, P.C., and Tonegawa, S. (1994). Altered peptidase and viral-specific T cell response in LMP2 mutant mice. Immunity *1*, 533–541. https://doi.org/10.1016/1074-7613(94)90043-4.
43. Basler, M., Beck, U., Kirk, C.J., and Groettrup, M. (2011). The Antiviral Immune Response in Mice Devoid of Immunoproteasome Activity. J. Immunol. *187*, 5548–5557. https://doi.org/10.4049/jimmunol.1101064.
44. Moebius, J., Van Den Broek, M., Groettrup, M., and Basler, M. (2010). Immunoproteasomes are essential for survival and expansion of T cells in virus-infected mice. Eur. J. Immunol. *40*, 3439–3449. https://doi.org/10.1002/eji.201040620.
45. Muchamuel, T., Basler, M., Aujay, M.A., Suzuki, E., Kalim, K.W., Lauer, C., Sylvain, C., Ring, E.R., Shields, J., Jiang, J., et al. (2009). A selective inhibitor of the immunoproteasome subunit LMP7 blocks cytokine production and attenuates progression of experimental arthritis. Nat. Med. *15*, 781–787. https://doi.org/10.1038/nm.1978.
46. Seifert, U., Bialy, L.P., Ebstein, F., Bech-Otschir, D., Voigt, A., Schröter, F., Prozorovski, T., Lange, N., Steffen, J., Rieger, M., et al. (2010). Immunoproteasomes Preserve Protein Homeostasis upon Interferon-Induced Oxidative Stress. Cell *142*, 613–624. https://doi.org/10.1016/j.cell.2010.07.036.
47. Kim, M., Serwa, R.A., Samluk, L., Suppanz, I., Kodroń, A., Stępkowski, T.M., Elancheliyan, P., Tsegaye, B., Oeljeklaus, S., Wasilewski, M., et al. (2023). Immunoproteasome-specific subunit PSMB9 induction is required to regulate cellular proteostasis upon mitochondrial dysfunction. Nat. Commun. *14*, 4092. https://doi.org/10.1038/s41467-023-39642-8.
48. Revy, P., Kannengiesser, C., and Fischer, A. (2019). Somatic genetic rescue in Mendelian haematopoietic diseases. Nat. Rev. Genet. *20*, 582–598. https://doi.org/10.1038/s41576-019-0139-x.
49. Buonocore, F., Kühnen, P., Suntharalingham, J.P., Del Valle, I., Digweed, M., Stachelscheid, H., Khajavi, N., Didi, M., Brady, A.F., Blankenstein, O., et al. (2017). Somatic mutations and progressive monosomy modify SAMD9-related phenotypes in humans. J. Clin. Invest. *127*, 1700–1713. https://doi.org/10.1172/JCI91913.
50. Crestani, E., Choo, S., Frugoni, F., Lee, Y.N., Richards, S., Smart, J., and Notarangelo, L.D. (2014). RAG1 Reversion Mosaicism in a Patient with Omenn Syndrome. J. Clin. Immunol. *34*, 551–554. https://doi.org/10.1007/s10875-014-0051-2.
51. Hirschhorn, R., Yang, D.R., Puck, J.M., Huie, M.L., Jiang, C.-K., and Kurlandsky, L.E. (1996). Spontaneous in vivo reversion to normal of an inherited mutation in a patient with adenosine deaminase deficiency. Nat. Genet. *13*, 290–295. https://doi.org/10.1038/ng0796-290.

The American Journal of Human Genetics, Volume *111*

Supplemental information

Expanding the PRAAS spectrum: *De novo* mutations of immunoproteasome subunit β-type 10 in six infants with SCID-Omenn syndrome

Caspar I. van der Made, Simone Kersten, Odelia Chorin, Karin R. Engelhardt, Gayatri Ramakrishnan, Helen Griffin, Ina Schim van der Loeff, Hanka Venselaar, Annick Raas Rothschild, Meirav Segev, Janneke H.M. Schuurs-Hoeijmakers, Tuomo Mantere, Rick Essers, Masoud Zamani Esteki, Amir L. Avital, Peh Sun Loo, Annet Simons, Rolph Pfundt, Adilia Warris, Marieke M. Seyger, Frank L. van de Veerdonk, Mihai G. Netea, Mary A. Slatter, Terry Flood, Andrew R. Gennery, Amos J. Simon, Atar Lev, Shirley Frizinsky, Ortal Barel, Mirjam van der Burg, Raz Somech, Sophie Hambleton, Stefanie S.V. Henriet, and Alexander Hoischen

Supplemental Note: Case Reports

Individual 1, born to non-consanguineous parents, presented at 8-weeks of age with generalized erythroderma with desquamation and bullae, mild diarrhea, lymphadenopathy and failure to thrive (length and weight – 2.5 SD). Laboratory investigations at presentation showed T cells within normal range for age, but 4 days later the individual developed T cell lymphopenia. There was a predominantly memory CD4+ CD45RO+ T cell population and near absent naïve CD4+ cells, cytotoxic CD8+ cells and B-cells, with normal NK cell numbers, resulting in SCID with Omenn syndrome-like features. Maternofetal transfusion was excluded as XX-maternal T lymphocytes were absent. There was a markedly reduced lymphocyte proliferation following mitogen stimulation and defective IgG, IgA and IgM production. Skin biopsy at diagnosis showed hyperparakeratosis, pronounced apoptotic keratinocytes surrounded by lymphocytes, and flat epidermis with vacuolization of basal epidermal layer. At that time no genetic diagnosis could be made and individuals' fibroblasts had normal sensitivity to radiation. Before the age of 3 months, the individual received an allogeneic HSCT from his HLA identical brother. SCT was complicated by graft-versus-host disease (GVHD) of the skin and intestine. The individual's immune cell subsets normalized post-HSCT with reconstitution of the entire T-cell repertoire, and B and NK cells. Three years post-HSCT, he developed encephalopathy, quadriplegia, and neurogenic bladder due to cyclosporine toxicity. A year later, treatment was complicated by a Parvovirus B19 infection with myocarditis and dilated cardiomyopathy. Any immunosuppressive treatment was stopped with complete resolution of cardiac function. In follow-up he shows excellent vaccination responses and remains completely immunocompetent. He is an emotionally strong young adult, with normal intelligence. Physically, beyond the consequences related to the history of cyclosporine toxicity, he continues to have infection- and drug-induced cutaneous hypersensitivity which, histologically, could not be correlated to any graft versus host disease.

Individual 2 was born following an uneventful pregnancy to healthy, non-consanguineous parents. He initially presented at two weeks following neonatal screening results of reduced TRECs (T-cell receptor excision circles) on Guthrie card. Physical examination was notable for thin sparse hair, a mild facial rash and mild dysmorphic facial features (protruding ears with pointed chin), adducted left thumb, hypospadias and micropenis. Initial testing showed a lack of T cells, with positive B cells on flow cytometry and a clonal T cell receptor repertoire. However, repeated testing revealed absent B cells in peripheral blood, and the phenotype was hence classified as a T-cell negative, B-cell negative and NK-cell positive SCID with an Omenn like phenotype. Treatment with preventive antibiotics and IVIG was commenced. At the age of one month the individual presented with CMV encephalitis and multisystem involvement, including seizures, and intractable diarrhea with consequent neurologic impairment manifesting as global developmental delay and multiple brain infarcts with diffuse brain atrophy. Over the next two years, he developed repeated CMV viremias, resistant to oral antiviral treatment. Additional

manifestations included pulmonary infections; intractable diarrhea, intermittently depending on total parenteral nutrition (TPN), hepatocellular and cholestatic liver failure with renal tubulopathy. Later on he presented with febrile episodes accompanied by marked leukocytosis suspected to be of auto-inflammatory origin responding to steroid treatment. Colonic biopsy revealed colitis with cryptitis and crypt abscesses with increased apoptotic debris and crypt attenuation with plasma cells (CD138 and CD38) within the lamina propria. CMV staining was negative. Skin biopsy revealed vacuolar interface dermatitis with eosinophils and pigment laden macrophages in the infiltrate. Although SCT was considered at an early stage, it was deferred to the age of 2.5 years at another institution by the family, and also due to his complex neurologic and CMV-related sequela. The individual died shortly after the procedure due to post transplant complications including transplant associated thrombotic micro-angiopathy (TMA).

Individual 3 was born at full term to healthy unrelated parents weighing 2.98kg. He was briefly observed on the neonatal intensive care unit because of possible meconium aspiration. Having been discharged well, he developed progressive watery diarrhoea from 3 weeks of age accompanied by an evolving rash. By 5 weeks of age he was below his birth weight with ongoing profuse diarrhoea, oral candidiasis and a generalised peeling and scaling erythroderma. His blood picture revealed eosinophilia and lymphopenia affecting all subsets; naive T cells and B cells were absent with residual T cells showing reduced T cell receptor diversity and impaired mitogen responses. The diagnosis of Omenn syndrome was made after excluding maternofetal engraftment, and supportive care including parenteral nutrition was provided. He received an unrelated umbilical cord transplant after reduced intensity conditioning using fludarabine and melphalan with alemtuzumab serotherapy. The peri-transplant course was stormy with severe sinusoidal obstruction syndrome and acute graft versus host disease of the skin, managed conventionally. Full donor chimerism persisted and there was partial immune reconstitution with sub-normal lymphocyte numbers but present humoral immune responses and no excess of infections. Nutritional rehabilitation could not be achieved and the individual went on to manifest a lifelong enteropathy requiring gastrostomy feeding, as well as chronic liver disease that was attributed to his SOS, and mild learning difficulties. In mid-childhood, he developed a mesangiocapillary glomerulonephritis that was refractory to immunosuppression and rapidly progressed to acute renal failure. He nonetheless stabilised on haemodialysis and eventually came to renal transplant but rejected this and eventually died of sepsis.

Individual 4 was born weighing 3.74kg after an uneventful pregnancy to healthy unrelated parents; two older half siblings were well. From 6 weeks of age, she developed severe seborrhoeic dermatitis that began on the scalp but spread to involve the entire body. She developed diarrhoea and oral candidiasis, both of which were persistent. By 3 months there was a superimposed vesicular rash that proved positive for VZV and she was admitted to hospital apparently septic. Pneumocystis jirovecii was subsequently

identified in bronchoalveolar lavage fluid. Immunological investigations were consistent with Omenn syndrome, showing absent B cells, normal NK cells and a very abnormal T cell compartment lacking naïve T cells and heavily skewed towards CD4 cells. Some IgM and IgA production were present. The individual was treated for her many infections and received myeloablative conditioning for a maternal haploidentical SCT as per contemporary practice. She tolerated this poorly, developing capillary leak syndrome with severe pneumonitis and subsequently GVHD of both skin and gut. Under immunosuppression she deteriorated neurologically despite ongoing antiviral therapy and sadly succumbed. Post mortem examination revealed VZV encephalitis.

Individual 5 was born weighing 3.43kg to unrelated healthy parents after a normal pregnancy; an elder sister was well. He manifested diarrhoea and weight loss from birth, rapidly developing a metabolic acidosis. By one month of age he was still below his birth weight despite parenteral nutrition and had reached our SCID referral unit via district and regional paediatric centres. His ongoing diarrhoea proved positive for adenovirus which was also present in the blood, associated with transaminitis. His blood picture was that of a leaky SCID with present IgM production despite very low lymphocyte numbers in all compartments, low numbers of naive T cells and poor PHA response despite high background T cell proliferation. A lymph node biopsy was grossly abnormal, with few lymphocytes and no mature follicles present. Within weeks he developed a maculopapular rash over the trunk, limbs and face consistent with Omenn syndrome. This individual received an unrelated donor cord transplant after reduced toxicity conditioning using treosulfan, fludarabine and alemtuzumab. He experienced considerable gut and skin toxicity which evolved into an inflammatory picture managed as acute GVHD. Although able to be discharged from hospital off parenteral nutrition, this individual had major problems sustaining his weight over the following years with waxing and waning enteropathy and skin rash. There was a partial response to immunosuppression and flaring of symptoms upon withdrawal, although not histologically typical of GVHD and associated with ongoing norovirus in stool. He did not sustain normal T cell numbers despite 100% donor chimerism, likely due to corticosteroid toxicity, and succumbed to sepsis aged 4 years.

Individual 6 was born at 38 weeks gestation following an elective Caesarean section for breech presentation. This is the parents' first child and parents are healthy and unrelated. The pregnancy was complicated by gestational diabetes. He was born weighing 3.57kg and was well at birth. He was identified as having SCID following newborn screening (low TRECs on day 5) and confirmatory lymphocyte subsets (T cell lymphopenia and absent naïve T cells). There was no evidence of maternofoetal engraftment. He was breastfed prior to the result of his NBS being known and was gaining weight appropriately. He was screened for infection (negative for respiratory, faecal and blood viruses), started on antimicrobial prophylaxis (fluconazole, co-trimoxazole) and palivizumab, and had tissue typing in anticipation of receiving a HSCT. He also received respiratory syncytial virus prophylaxis

with palivizumab. Given his age and the NBS result he did not receive any vaccinations. Clinical exome sequencing followed by targeted analysis of known and candidate genes identified a variant in *PSMB10*. Capillary sequencing of patient and parental genomic DNA confirmed this to be *de novo* in origin. T cell proliferation was diminished in individual 6 compared to control in response to phytohaemagglutinin (PHA), phorbol myristate acetate (PMA) and CD3 stimulation. He had normal T cell receptor Vβ chain usage, as assessed by flow cytometry. He was admitted for HSCT at 8 weeks of age and at this point was noted to have some blood and mucus mixed in with his stools. Individual 6 received a parental haploidentical TCRαβ/CD19 depleted transplant after a conditioning regimen containing antithymocyte globulin (ATG), rituximab, treosulfan and fludarabine. He tolerated conditioning well with minimal gut toxicity (he did not require any parenteral nutrition) but developed a transient erythema multiforme-like skin rash two weeks after receiving his transplant (HSV, enterovirus, mycoplasma negative) which resolved after stopping tazocin and co-trimoxazole. He engrafted with 100% donor chimerism and was well until 1 month post-transplant, when he developed new unexplained vomiting rapidly (hours) followed by a significant neurological deterioration with reduced level of consciousness, increased tone and seizures. Urgent magnetic resonance imaging revealed T2 hyperintensity involving the white matter extending from the perirolandic region to the internal and external capsules, temporal lobes, thalami, lentiform nucleus and pons. Intracranial arteries were patent. Cerebrospinal fluid showed elevated protein (2.24g/L) but was paucicellular and free of pathogens by culture, PCR and metagenomic analysis; autoantibodies were also negative. Whilst covering for infection with meropenem and aciclovir, this episode was managed with high dose corticosteroids as well as full supportive care including respiratory support, anticonvulsants and muscle relaxants, with partial recovery. Individual 6 is currently approximately 2 months post HSCT and has been discharged from hospital on levetiracetam, clonidine, baclofen, diazepam and a weaning dose of steroid. He is now smiling, fixing and following again. A repeat MRI showed maturation and some improvement of the previously identified white matter changes.

Supplemental Figures

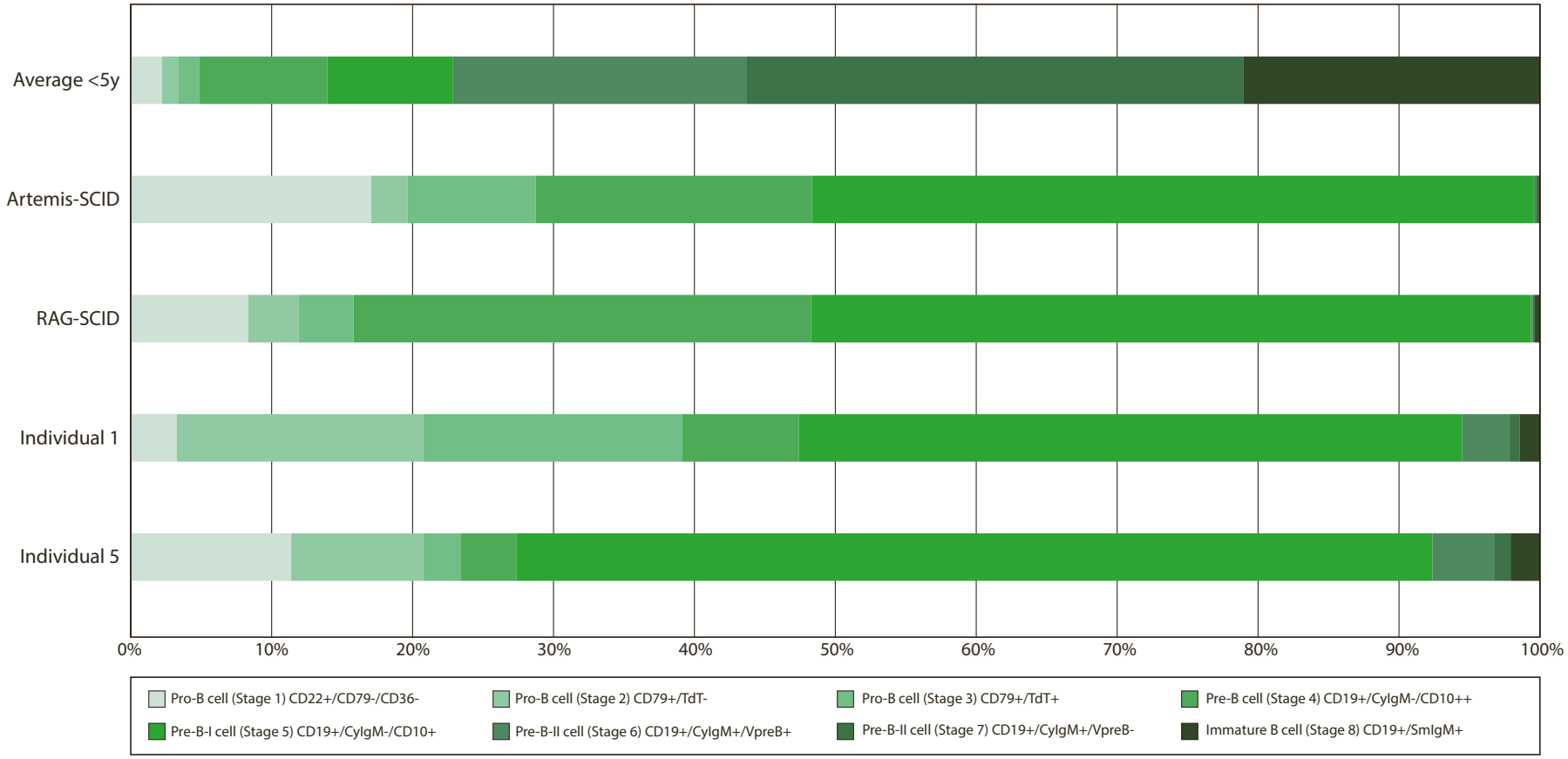

Figure S1. Composition of bone marrow precursor B-cell compartment.
B cell developmental stages were determined by flow cytometry on bone marrow biopsies obtained from individuals 1 and 5 and compared to healthy individuals <5y (n=9) and individuals with Omenn syndrome caused by Artemis deficiency (n=7) and RAG deficiency (n=17). All numbers are shown as percentages of the total measured B cells and have been corrected for blood contamination.

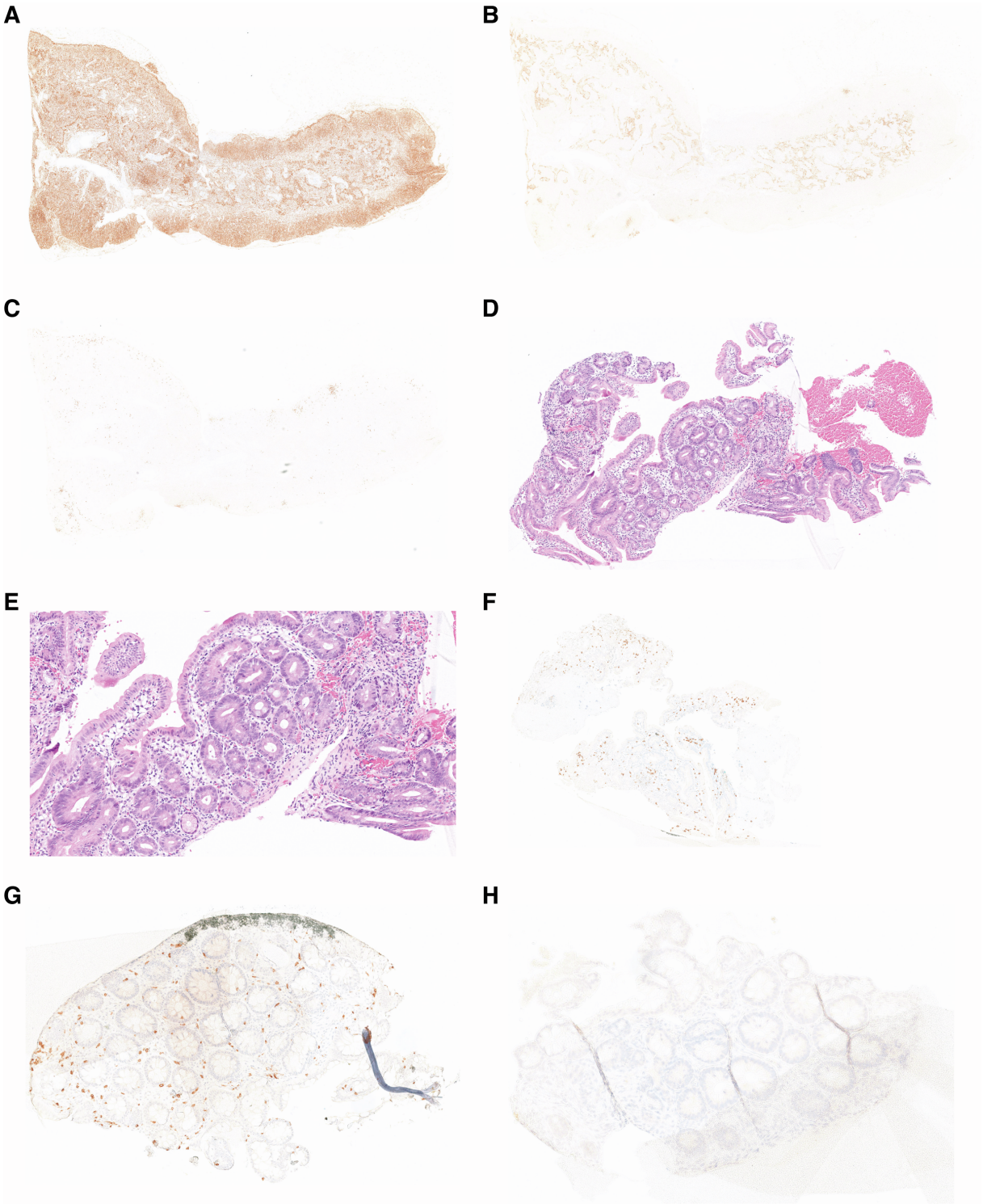

Figure S2. Histopathological evaluation of tissue biopsies.
(A-C) Immunohistochemistry of the inguinal lymph node from individual 5 showed a reduced number of T cells with a CD4+ majority (A) and small underlying CD21+ follicular dendritic cell meshworks (B) with sparse aggregates of CD79+ B-cells (C) associated with abortive primary follicle formation. There were no germinal centers. A small bowel biopsy from individual 5 showed focal villous atrophy (D) with increased mitosis and apoptotic bodies in the crypts (E) and reduced numbers of CD3+ T lymphocytes (F). Immunohistochemistry of the colon mucosa from individual 5 also indicated a reduced number of CD3+ T lymphocytes (G) and absent CD79+ plasma cells (H).

	Individual 1	Individual 2	Individual 3	Individual 4	Individual 5	Individual 6
Ancestry	European	Jewish Sepharadi	European	European	European	European
Mutation	c.601G>A; p.Gly201Arg	c.601G>A; p.Gly201Arg	c.601G>C; p.Gly201Arg	c.601G>A; p.Gly201Arg	c.166G>C; p.Asp56His	c.166G>C; p.Asp56His
Allele frequency[a]	0	0	0	0	0	0
CADD score	35	35	34	35	28	35
Age at investigation (w)	8	2	6	13	4	0
Sex	M	M	M	F	M	M
Clinical presentation	SCID/Omenn syndrome FTT, mild diarrhoea, skin rash, oral thrush, lymphadenopathy	SCID/Omenn FTT, severe diarrhoea, skin rash, intermittend TPN-dependent, hepatocellular and cholestatic liver failure with renal tubulopathy	SCID/Omenn syndrome FTT, diarrhoea, skin rash, oral thrush	SCID/Omenn syndrome FTT, skin rash, vesicular rash, oral thrush	SCID/Omenn syndrome FTT, severe diarrhoea, skin rash, disseminated adenovirus, TPN-dependent with elevated ALT	Newborn screening
Rash	Generalised erythroderma with desquamation and bullae.	Mild facial rash evolving into an erythematous papular rash with hyperpigmented macules	Generalised erythroderma with peeling	Thickened red skin with super-imposed crusting vesicular rash (VZV+)	Raised maculopapular rash on trunk, limbs and face, managed as OS with topical corticosteroid	Slightly rough erythematous rash to abdomen and chest
Age at onset of rash (w)	< 1	2	3	1	8	<1
Alopecia (hair loss)	Loss of hair between birth and clinical presentation with progression to total alopecia	Sparse hair	Sparse hair	Sparse hair	-	-
Hepatomegaly	-	-	1cm	2cm	-	-
Infection and inflammation	Oral candidiasis, secondary skin infection (S. aureus) Otitis media	CMV encephalitis and multi-organ involvement (4w of age), multiple episodes of respiratory insufficiency	Oral candidiasis Septic episode pre-transplant	Oral candidiasis Chronic VZV PCP on BAL Ear discharge (otitis media?)	Disseminated adenovirus	-

		requiring prolonged mechanical ventilation. Recurrent episode of systemic inflammation responsive to steroids				
Dysmorphology	Overfolded helices, hypoplasia alea nasi, cone-shaped teeth, hypodontia	Mild dysmorphic facial features (protruding ears with pointed chin), adducted left thumb, hypospadias and micropenis. Dysplastic nails.	No	No	No	No

Table S1. Extended genetic and clinical information.

[a] Allele frequency in GnomAD, dbSNP or ExAC databases.

ALT, alanine aminotransferase; BAL, broncheo-alveolar lavage; CADD, combined annotation dependent depletion; CMV, cytomegalovirus; FTT, failure to thrive; OS, Omenn Syndrome; PCP, pneumonia due to *Pneumocystis jirovecii*; SCID, severe combined immunodeficiency; TPN, total-parenteral nutrition; VZV, varicella zoster virus

	Individual 1	Individual 2	Individual 3	Individual 4	Individual 5	Individual 6
Age at investigation (w)	8	2	6	12	4	2
Eosinophils (/µl) (40-800)	896	2930	1700	1700	720	1000
IgG (g/L) (3.7-12.6)	1.35	0.974	2.6	2.76	5.1	2.4
IgA (g/L) (0.02-0.15)	< 0.07	< 0.01	<0.07	0.23	0.41	<0.04
IgM (g/L) (0.05-0.29)	< 0.07	< 0.02	0.09	0.12	0.98	<0.04
CD3 (/µl) (1700-3600)	1300	1552	595	1239	188	309
CD4 (/µl) (1700-2800)	1100	730	551	1143	137	272
CD8 (/µl) (800-1200)	40	820	72	83	26	60
CD4:CD8 ratio	27.5	0.89	7.7	13.8	5.3	4.5
CD19 (/µl) (500-1500) (%)	40	430 (disappeared shortly after presentation)	0	<1	19	34
CD16/CD56 (/µl) (300-700)	70	1826	46	414	22	368
CD45RA (%CD3)	8.6	NA[a]	NA	0	8 (CD45RA+CD27+)	0
CD45RO (%CD3)	95	NA[a]	91	NA	NA	4
TCR αβ (%CD3)	98	NA	97	99	74	96
TCR γδ (%CD3)	2	NA	3	1	26	4
PHA stimulation index (control)	PHA 10900 cpm (ref. > = 17000)	Limited TCR repertoire with decreased mitogen response	10 (415)	3 (238)	10 (418)	31
PHA counts individual (control)	NA	NA	16558 (85097)[c]	NA	52976[c] (69434)	130
Skin (biopsy)	Hyperparakeratosis, pronounced apoptotic keratinocytes surrounded by lymphocytes, flat epidermis with vacuolization of basal epidermal layer[b]	Vacuolar interface dermatitis with eosinophils and pigment laden macrophages in the infiltrate	Flattened epidermis with widespread basal vacuolation. Eosinophilic keratinocytes with pyknotic nuclei are seen within the epidermis, some associated with adjacent lymphocytes – the features of satellite cell necrosis. The superficial dermis contains a moderate perivascular chronic inflammatory cell infiltrate. The features are those of lichenoid inflammation and essentially identical to GVHD grade 2	NA	NA	NA
Lymph node (biopsy)	-	-	-	-	Paucicellular, stroma-rich	-

					lymph node with moderate numbers of interdigitating dendritic cells/Langerhans cells and eosinophils, but the nodular and diffuse "dermatopathic" changes characteristically seen in OS are not present. The vast majority of T cells present are CD4+ cells. Occasional large CD30+ cells, most likely activated T cells, are present. The few B cells associated with FDC meshworks are shown to be IgD+, consistent with abortive primary follicles.	
Bone marrow (aspirate)	Block in B cell maturation	-	-	-	Block in B cell maturation	-
Gastrointestinal tract (endoscopy, biopsy)	-	Colonic biopsy: colitis with cryptitis and crypt abscesses with increased apoptotic debris and crypt attenuation with plasma cells (CD138 and CD38) within the lamina propria.	Upper GI endoscopy and biopsy: Partial villous atrophy. Nodular macroscopic appearance of jejunum. CD3-CD4+ cells present; no T cells.	-	Pre-transplant GI endoscopy: consistent with immuno-deficiency related enteropathy	-
Other	In the skin biopsy before HSCT two clonal TCRG gene rearrangements were detected, indicating the presence of a biallelic rearranged clonal T-cell population (*)	TCR Vb repertoire analysis showed clonal expansions of two VbR's: Vb3, Vb) and lack of most other VbR's, suggestive of autoreactive clonal expansion as seen in individuals with SCID and OS.	TCR Vb usage: 73% of CD3 pos cells were pos for TCRVB families tested with increase in TCRVB2 and TCRVB14 and absent TCRVB11, 16, 18, 23 and 24 families. Clonal TCR rearrangements detected (TCRVBJA, VBJB, TCRVGJB and TCRD)	NA	NA	Normal Vb usage (CD3+CD4+ and CD3+CD4-)

Table S2. Extended laboratory and histopathological information.

Laboratory parameters are presented with units and normal reference ranges if applicable.

[a] For this individual TREC copies were available with significantly reduced levels (179 with reduction to 5 over time).

[b] Previously published in D'Hauw et al. British Journal of Dermatology 2008[1].

[c] High background in individual

FDC, follicular dendritic cell; GVHD, graft-versus-host-disease; NA, not assessed; OS, Omenn Syndrome; PHA, phytohaemagglutinin; SCID, severe combined immunodeficiency; TCR, T cell receptor;

	Individual 1	Individual 2	Individual 3	Individual 4	Individual 5	Individual 6
Age at transplantation (w)	12	130	11	16	12	8
Materno-fetal engraftment	EXCLUDED by X-Y FISH and microsatellite markers	-	EXCLUDED by X-Y FISH and microsatellite markers	-	-	Excluded by microsatellite markers
Donor information	10/10 HLA identical sibling	ATG	URD	Maternal haplo	9/10 mM cord blood	Paternal haplo
Serotherapy	ATG 5 mg/kg	Cyclosporine + MMF	alemtuzumab	ATG 6 mg/kg	None	ATG 5mg/kg, Rituximab 20mg/m2
Chemotherapy	CsA	Engraftment failure, pancytopenia	Flu mel	Bu 4 mg/kg, cyclo 200 mg/kg	Treo 36 g/m2, Flu 150 mg/m2	Treo 10g/m^2, Flu 40mg/m^2
Outcome	100% donor	ATG	100% donor	-	100% donor	-
Post-HSCT complications	Severe skin and gut GvHD	Post-transplant complications incl. transplant associated TMA, sepsis with multi-organ failure	Skin GVHD Severe VOD	Pneumonitis with capillary leak peri-engraftment GVHD skin and gut Hypertension Recurrence of VZV with fatal encephalo-pathy	Skin GVHD with late recurrence (12m), steroid-sensitive Marked mucositis and skin toxicity Adeno-viraemia Liver dysfunction with marked ductular cholestasis on biopsy	Acute leuko-encephalo-pathy
Follow-up	Alive, 18 yrs post HSCT Encephalo-pathy, quadriplegia and neurogenic bladder due to CsA toxicity Parvovirus B19 Myocarditis Osteoporosis Kerato-	Died post-HSCT (131 weeks)	Died age 16 yrs Long term enteropathy Liver cirrhosis with varices Mesangiocapil lary GN with acute renal failure, ESRD requiring dialysis (and rejected renal allograft)	Died post-HSCT (11w)	Died age 4 yrs Sudden profound hypo-thyroidism Long term enteropathy FTT with norovirus infections, managed with immune-suppression, flares during	Alive, 2m post-HSCT

	conjunctivitis sicca Marked sensitive and hyper-responsive skin in response to infections and certain drugs		Learning difficulties		tapering, died due to recurrent infections	

Table S3. Extended information on hematopoietic stem cell transplantation therapy
ATG, antithymocyte globulin; Bu, busulfan; CsA, cyclosporin; Cyclo, cyclophosphamide; ESRD, end-stage renal disease; Flu, fludarabine; FTT, failure to thrive; GN, glomerulonephritis; GVHD, graft-versus-host-disease; Mel, melphalan; MMF, mycophenolate mofetil; TMA, thrombotic micro-angiopathy; Treo, treosulfan; VOD, veno-occlusive disease; VZV, varicella zoster virus

	Individual 1	**Individual 2**	**Individual 3**	**Individual 4**	**Individual 5**	**Individual 6**
Candidate variants within the IEI panel	*FLG* (Chr1:g.152285861G>A NM_002016: c.1501C>T, p.(Arg501Ter))	-	-	-	*TNFSF12* (Chr17:746063 3T>C NM_003809.3: c.716T>C, p.(Phe239Ser)	-[a]
Possible *de novo* variants (if trio analysis was performed)	*PSMB10* (Chr16:g.67968809C>T; NM_002801: c.601G>A p.(Gly201Arg))	*PSMB10* (Chr16:g.67968809C>T; NM_002801: c.601G>A p.(Gly201Arg))	-	-	-	*PSMB10* (Chr16:g.67968809C>T; NM_002801: c.601G>A p.(Gly201Arg)) on prospective screening
	CCNE1 (Chr19:g.30314571C>T; NM_001238.4: c.1120C>T, p.(Arg374Ter))	*SLC30A5* (Chr5:g.68413208G>A; NM_022902: c.1424G>A, p.Arg475Gln)	-	-	-	-

Table S4. Candidate variants remaining after WES filtering
[a] None within NHS Genomics England Panel for Primary immunodeficiency or monogenic inflammatory bowel disease (V4.0) (https://panelapp.genomicsengland.co.uk/panels/398)

Subjects & methods

Study participants and ethics approval

Individual 1 was referred to the Department of Pediatrics at the Radboud University Medical Center at 8 weeks of age. Individual 2 presented to the Pediatric Immunology Unit at the Sheba Medical Center after abnormal newborn screening raising suspicion of severe combined immunodeficiency (SCID). Written informed consent and publication consent were obtained from individuals and/or their parents and were approved by the local Ethics Committees. Individuals 3-6 were referred to the Paediatric Immunology and haemotopoietic stem cell transplantation (HSCT) team at the Great North Children's Hospital (or its predecessor, Newcastle General Hospital) in Newcastle upon Tyne. Their parents provided generic consent for future research through ethically approved procedures (REC reference 10/H0906/22 or 20/NE/0044).

Whole-exome sequencing analysis

Clinical whole-exome sequencing was performed on genomic DNA extracted from whole blood of individuals 1-2 and their parents according to standard hospital procedures. Individuals 3-5 underwent whole exome sequencing retrospectively and as singletons using dermal fibroblast (individuals 3 and 4) or whole blood (individual 5) genomic DNA as a research procedure. Coding regions were enriched using the *SureSelect Human All Exon V5 Kit (Agilent, Santa Clara, United States)* and sequenced on the Illumina HiSeq platform (HiSeq 4000 for individual 1, HiSeq 2500 for individuals 2-5; Illumina Inc., San Diego, CA, United States; AROS (Applied Biotechnology AS, Denmark)). Sequence reads were aligned to the human reference genome (hg19) with the Burrows-Wheeler Aligner Algorithm and variants were called using the HaploTypeCaller algorithm of GATK. For all individuals, in-house custom analysis pipelines were applied for variant annotation.[2] KGG-seq v.08 was used for annotation of identified variants in individual 2. Variant were first prioritized in a diagnostic setting by filtering for coding, nonsynonymous variants with allele frequencies below 1% in the in-house database or population databases (dbSNP ExAC and GnomAD) in genes included in the *in silico* gene panel for inborn errors of immunity. Subsequently, downstream filtering was performed to retain rare variants (MAF <0.1%) variants with a minimum of 5 variant reads and >20% variation and *de novo* status using the DeNovoCheck tool (**Table S4**). More technical details for individual 1 can be retrieved from a previously published series of individual-parent exome trio sequencing for inborn errors of immunity, that included this individual.[3] Moreover, nucleotide conservation (PhyloP[4]) and *in silico* pathogenicity predictors, *i.e.* PolyPhen2,[5] SIFT,[6] Mutation Taster,[7] PROVEAN,[8] Mutation Assessor[9] and CADD_Phred[10] were used for variant prioritization. Individual 6 was identified following newborn screening as having low TRECs. Subsequent clinical whole exome sequencing was negative against NHS England's primary immunodeficiency gene panel (R15) but targeted research analysis identified a variant in *PSMB10*.

Genome-wide SNP array

SNP-array analysis was performed in individual 1 to identify copy-number variants and regions of altered B-allele frequency including regions of (somatic) homozygosity as described previously.[11] Chromosomal SNP-based microarray was conducted for individual 2 on a Baylor medical genetics laboratories targeted postnatal oligo v8.1.1 platform, returning a normal result.

Sanger and amplicon sequencing

The *de novo* status of the identified *PSMB10* variants was determined in trio-WES data (Individuals 1 and 2) or assessed by standard Sanger sequencing (Individuals 3-6). All available parental samples (11 of 12) were wild type. In individual 1, deep amplicon sequencing was performed as previously described,[12] enabling accurate identification of the variant allele fractions (VAF) across the two different tissue samples.

Somatic UPD/RM calling in exome data

To estimate the level of mosaicism, *i.e.* proportion of abnormal cells with (segmental) chromosomal abnormalities, as well as their parental origin, we applied haplarithmisis[13] as previously described[14] with some modifications to adapt our approach for WES. Briefly, we applied haplotypecaller from the GATK tool haplotypecaller[15] to determine SNVs annotated in the dbSNP database (version 150). Subsequently, using the R-function extract.gt (vcfR package bioconductor), depth of coverage of each genomic location was calculated per sample and BAF values were determined. We then applied trio analysis option of haplarithmisis for determining parental haplarithms, and QDNAseq for determining logR-values per 10kb bins.[16] We then estimated the level of mosaicism by calculating the distortion of segmented haplarithm values from the expected 1:1 allelic ratio, i.e., 0.5:0.5 vertical distance in each segmented parental haplarithms.

Structural modelling

The structural impact of the p.(Asp56His) and p.(Gly201Arg) variants in *PSMB10* were modelled using experimentally determined 3D structures of the 20S proteasome (PDB: 6E5B), as well as its 26S proteasome homologue (PDB: 6MSB). Variants in the TUB6 mouse model, p.(Gly170Trp) and the p.(Gly201Arg) equivalent, were modelled into the crystal structure of mouse 20S proteasome (PDB: 3UNH). Changes in protein stabilities upon mutations were estimated using FoldX energy function (v.5.0).[17] For a given mutation, structural models were constructed using RepairPDB and BuildModel functions with 5 iterations of sidechain rotamer adjustments, followed by calculation of average of the differences in free energies between wildtype and the mutant structures in kcal/mol.

Immunoblotting

Primary dermal fibroblasts at low passage number were seeded at 100,000 per well of 6-well plate and treated, or not, with interferon-gamma at 200 IU/ml (Immunikin, Boehringer Ingelheim, Germany) for 48 hrs. Each well was washed with PBS and lysed using radio-immunoprecipitation assay buffer (RIPA; 150mM sodium chloride, 1% Triton X-100, 0.5% sodium deoxycholate, 0.1% sodium dodecyl sulphate, 50mM Tris pH7.4) supplemented with cOmplete™ Protease Inhibitor Cocktail and PhosSTOP™ Phosphatase inhibitor Cocktail (Roche, Switzerland). Lysates were denatured at 70°C for 15 minutes with 10% dithiothreitol (DTT), and 1X NuPAGE LDS Sample Buffer (Thermo Fisher Scientific, USA) then loaded on to 4-12% Bis-Tris gel alongside pre-stained protein ladder (PageRuler Plus, Thermo Fisher Scientific, USA) for gel electrophoresis in 1X NuPAGE MOPS SDS Running Buffer (Invitrogen, USA). An equal volume of lysate was loaded per lane. Proteins were transferred to 0.45mM polyvinyl difluoride (PVDF) membranes (Millipore, USA) at 20V using 1X NuPAGE Transfer Buffer (Invitrogen, USA) in 20% methanol. Membranes were blocked for 60 minutes using 5% bovine serum albumin in tris-buffered saline with 0.1% Tween (TBS-T) prior to immunostaining. Membranes were incubated overnight with anti-PSMB10 and anti-alpha-Tubulin primary antibodies (PSMB10/MECL-1 (E6R7O) Rabbit mAb #17579 (final concentration: 1:1000) and alpha-Tubulin (DM1A) mouse mAb #3873 (final concentration 1:10,000) from Cell Signaling Technology) followed by washing and incubation with anti-rabbit-IgG-HRP and anti-mouse-IgG-HRP secondary antibodies (final concentrations: 1:5000; #7074S and #7076S respectively, Cell Signaling Technology). Membranes were developed with Immobilon ECL substrate (Millipore, USA) and chemiluminescent images were visualized with the LI-COR Odyssey (LI-COR, USA).

Supplemental references

1. D'hauw, A., Seyger, M.M.B., Groenen, P.J.T.A., Weemaes, C.M.R., Warris, A., and Blokx, W.A.M. (2008). Cutaneous graft-versus-host-like histology in childhood. Importance of clonality analysis in differential diagnosis. A case report. Br J Dermatol *158*, 1153–1156. 10.1111/j.1365-2133.2008.08497.x.
2. De Ligt, J., Willemsen, M.H., Van Bon, B.W.M., Kleefstra, T., Yntema, H.G., Kroes, T., Vulto-van Silfhout, A.T., Koolen, D.A., De Vries, P., Gilissen, C., et al. (2012). Diagnostic Exome Sequencing in Persons with Severe Intellectual Disability. N Engl J Med *367*, 1921–1929. 10.1056/NEJMoa1206524.
3. Hebert, A., Simons, A., Schuurs-Hoeijmakers, J.H., Koenen, H.J., Zonneveld-Huijssoon, E., Henriet, S.S., Schatorjé, E.J., Hoppenreijs, E.P., Leenders, E.K., Janssen, E.J., et al. (2022). Trio-based whole exome sequencing in patients with suspected sporadic inborn errors of immunity: a retrospective cohort study. eLife. 10.7554/eLife.78469.
4. Pollard, K.S., Hubisz, M.J., Rosenbloom, K.R., and Siepel, A. (2010). Detection of nonneutral substitution rates on mammalian phylogenies. Genome Res. *20*, 110–121. 10.1101/gr.097857.109.
5. Adzhubei, I.A., Schmidt, S., Peshkin, L., Ramensky, V.E., Gerasimova, A., Bork, P., Kondrashov, A.S., and Sunyaev, S.R. (2010). A method and server for predicting damaging missense mutations. Nat Methods *7*, 248–249. 10.1038/nmeth0410-248.
6. Vaser, R., Adusumalli, S., Leng, S.N., Sikic, M., and Ng, P.C. (2016). SIFT missense predictions for genomes. Nat Protoc *11*, 1–9. 10.1038/nprot.2015.123.
7. Schwarz, J.M., Cooper, D.N., Schuelke, M., and Seelow, D. (2014). MutationTaster2: mutation prediction for the deep-sequencing age. Nat Methods *11*, 361–362. 10.1038/nmeth.2890.
8. Choi, Y., Sims, G.E., Murphy, S., Miller, J.R., and Chan, A.P. (2012). Predicting the Functional Effect of Amino Acid Substitutions and Indels. PLoS ONE *7*, e46688. 10.1371/journal.pone.0046688.
9. Reva, B., Antipin, Y., and Sander, C. (2011). Predicting the functional impact of protein mutations: application to cancer genomics. Nucleic Acids Research *39*, e118. 10.1093/nar/gkr407.
10. Rentzsch, P., Witten, D., Cooper, G.M., Shendure, J., and Kircher, M. (2019). CADD: predicting the deleteriousness of variants throughout the human genome. Nucleic Acids Research *47*, D886–D894. 10.1093/nar/gky1016.
11. Jongmans, M.C.J., Verwiel, E.T.P., Heijdra, Y., Vulliamy, T., Kamping, E.J., Hehir-Kwa, J.Y., Bongers, E.M.H.F., Pfundt, R., van Emst, L., van Leeuwen, F.N., et al. (2012). Revertant Somatic Mosaicism by Mitotic Recombination in Dyskeratosis Congenita. The American Journal of Human Genetics *90*, 426–433. 10.1016/j.ajhg.2012.01.004.
12. Acuna-Hidalgo, R., Sengul, H., Steehouwer, M., Vorst, M. van de, Vermeulen, S.H., Kiemeney, L.A.L.M., Veltman, J.A., Gilissen, C., and Hoischen, A. (2017). Ultra-sensitive Sequencing Identifies High Prevalence of Clonal Hematopoiesis-Associated Mutations throughout Adult Life. The American Journal of Human Genetics *101*, 50–64. 10.1016/j.ajhg.2017.05.013.
13. Zamani Esteki, M., Dimitriadou, E., Mateiu, L., Melotte, C., Van der Aa, N., Kumar, P., Das, R., Theunis, K., Cheng, J., Legius, E., et al. (2015). Concurrent Whole-Genome Haplotyping and Copy-Number Profiling of Single Cells. The American Journal of Human Genetics *96*, 894–912. 10.1016/j.ajhg.2015.04.011.
14. Zamani Esteki, M., Viltrop, T., Tšuiko, O., Tiirats, A., Koel, M., Nõukas, M., Žilina, O., Teearu, K., Marjonen, H., Kahila, H., et al. (2019). In vitro fertilization does not increase the incidence of de novo copy number alterations in fetal and placental lineages. Nat Med *25*, 1699–1705. 10.1038/s41591-019-0620-2.
15. McKenna, A., Hanna, M., Banks, E., Sivachenko, A., Cibulskis, K., Kernytsky, A., Garimella, K., Altshuler, D., Gabriel, S., Daly, M., et al. (2010). The Genome Analysis Toolkit: A MapReduce framework for analyzing next-generation DNA sequencing data. Genome Res. *20*, 1297–1303. 10.1101/gr.107524.110.
16. Scheinin, I., Sie, D., Bengtsson, H., Van De Wiel, M.A., Olshen, A.B., Van Thuijl, H.F., Van Essen, H.F., Eijk, P.P., Rustenburg, F., Meijer, G.A., et al. (2014). DNA copy number analysis of fresh and formalin-fixed specimens by shallow whole-genome sequencing with identification and

exclusion of problematic regions in the genome assembly. Genome Res. *24*, 2022–2032. 10.1101/gr.175141.114.
17. Schymkowitz, J., Borg, J., Stricher, F., Nys, R., Rousseau, F., and Serrano, L. (2005). The FoldX web server: an online force field. Nucleic Acids Research *33*, W382–W388. 10.1093/nar/gki387.